

1 **HETEROGENEOUS OPTIMIZED SCHWARZ METHODS FOR**
2 **SECOND ORDER ELLIPTIC PDES**

3 MARTIN J. GANDER* AND TOMMASO VANZAN†

4 **Abstract.** Due to their property of convergence in the absence of overlap, optimized Schwarz
5 methods are the natural domain decomposition framework for heterogeneous problems, where the
6 spatial decomposition is provided by the multi-physics of the phenomena. We study here heteroge-
7 neous problems which arise from the coupling of second order elliptic PDEs. Theoretical results and
8 asymptotic formulas are proposed solving the corresponding min-max problems both for single and
9 double sided optimizations, while numerical results confirm the effectiveness of our approach even
10 when analytical conclusions are not available. Our analysis shows that optimized Schwarz methods
11 do not suffer the heterogeneity, it is the opposite, they are faster the stronger the heterogeneity is.
12 It is even possible to have h independent convergence choosing two independent Robin parameters.
13 This property was proved for a Laplace equation with discontinuous coefficients, but only conjectured
14 for more general couplings in [12]. Our study is completed by an application to a contaminant
15 transport problem.

16 **Key words.** Optimized Schwarz Methods - Heterogeneous Domain Decomposition Methods -
17 Optimized Transmission Conditions - Contaminant Transport

18 **AMS subject classifications.** 65N55, 65N22, 65F10, 65F08

19 **1. Introduction.** The classical Schwarz method is a domain decomposition al-
20 gorithm for solving large scale PDEs. It consists in dividing the domain of computa-
21 tion into many subdomains, solving iteratively the local problems while exchanging
22 information along the interfaces through Dirichlet boundary conditions. The pioneer-
23 ing paper [25], in which Lions proposed a convergent algorithm using Robin transmis-
24 sion conditions, paved the way to the development of the optimized Schwarz methods
25 which exploit optimized transmission conditions in order to overcome some of the
26 drawbacks of the classical Schwarz method such as slow convergence and overlap re-
27 quirement [10]. The procedure to obtain such optimized transmission conditions is
28 now well established [9]: the problem of interest is posed in a simplified setting where
29 one can use the Fourier transform, for unbounded domains, or Fourier series expansion
30 or more generally separation of variables [19, 18], for bounded domains, to transform
31 the PDE into a set of ODEs parametrized by the frequencies k . Then, solving the
32 ODEs and using the transmission conditions, one can get a recursive relation for
33 the Fourier coefficients and obtain a closed formula for the convergence factor which
34 contains some free parameters to optimize.

35 The literature regarding optimized Schwarz methods for homogeneous problems
36 is well developed. Optimized transmission conditions have been obtained for many
37 problems such as Helmholtz equations [16, 14], Maxwell equations [4, 22, 30], advec-
38 tion diffusion problems [8, 18], Navier Stokes equations [3], shallow water equations
39 [27] and Euler equations [6]. In all the previous work, homogeneous problems are
40 analyzed, in the sense that a unique physics is considered in the whole domain, and
41 therefore the coupling on the interfaces regards equations of the same nature. First
42 attempts to generalize this situation have been carried out in [26], [12], where Laplace
43 equations with different diffusion coefficients were considered, and in [5], which was

*Section de mathématiques, Université de Genève, 2-4 rue du Lièvre, Genève (martin.gander@unige.ch).

†Section de mathématiques, Université de Genève, 2-4 rue du Lièvre, Genève (tomaso.vanzan@unige.ch).

44 devoted to Maxwell equations with discontinuous coefficients. Let us remark that at
45 least two possible interpretations of heterogeneous domain decomposition methods
46 exist. The first one concerns problems where the same physical phenomenon is taking
47 place in the whole domain, but it can be convenient to use a cheaper approximation
48 in some parts of the domain in order to save computational resources. This might
49 be the case in the presence of boundary layers, or for example in CFD simulations
50 where a potential flow is used far away from the zone of interest while the Navier-
51 Stokes equations are fully solved near, for instance, an aircraft. In this situation, good
52 transmission conditions can be obtained through a factorization approach, see [15] for
53 further details.

54 In this manuscript we follow the second interpretation which assumes that two
55 different physical phenomena are present in the domain and they interact through an
56 interface. In this case some physical coupling conditions must be satisfied along the
57 common interface, such as the continuity of the function and its normal derivative for
58 second order PDEs, or the continuity of normal stresses for fluid-structure problems.
59 Some examples in this direction can be found in [17], where optimized transmission
60 conditions were obtained for the coupling between the hard to solve Helmholtz equa-
61 tion and the Laplace equation, or in [21] where a partial optimization procedure was
62 carried out for a fluid-structure problem. For this kind of heterogeneous problems,
63 a domain decomposition approach can be extremely useful since it allows to reuse
64 specific solvers designed for the different physics phenomena present in the domain.
65 For instance, one can use a finite volume solver where a strong advection is present
66 while using a multigrid solver where diffusion dominates or an ad-hoc linear elas-
67 ticity solver combined with a CFD code for the Navier-Stokes equations. In this
68 perspective, optimized Schwarz methods lead to a significantly better convergence of
69 the coupling routine with respect to other domain decomposition algorithms (e.g.
70 Dirichlet-Neumann, Robin-Neumann) since they take into account the physical prop-
71 erties in their transmission conditions. We refer the interested reader to [23, 24] for
72 the application of optimized Schwarz methods for the coupling of atmospheric and
73 oceanic computational simulation models.

74 We study here first the coupling between a reaction diffusion equation and a dif-
75 fusion equation and second the harder coupling between a general second order PDE
76 and a reaction diffusion equation. We provide theoretical results and asymptotic for-
77 mulas for the optimized parameters, and we show the effectiveness through numerical
78 simulations. The manuscript is completed by the application of our results to a phys-
79 ical model describing contaminant transport in underground media, which is a topic
80 of great interest in the last thirty years due, for instance, to the increasing threat of
81 contamination of groundwater supplies by waste treatments and landfill sites or to
82 the disposal of nuclear radioactive waste [2]. We refer to [1] for a reference regarding
83 modeling issues of contaminant transport. Our model assumes that the computa-
84 tional domain $\Omega = \Omega_1 \cup \Omega_2 \cup \Omega_3 \cup \Omega_4$, represented in Figure 1, can be partitioned
85 into four layers. In the first one, the contaminant, whose concentration is described
86 through the unknown u , penetrates mainly thanks to rainfalls and therefore an ad-
87 vection towards the negative y direction is present. The next two layers are formed
88 by porous media so that the contaminant spreads in a diffusive regime described by
89 the Laplace equation. We furthermore suppose that in the second layer, some chem-
90 ical reactions may take place which are synthesized in the reaction term. Finally in
91 the last layer, an underground flow transports the contaminant in the x direction to-
92 wards a groundwater supply which is connected to a water well. The problem belongs
93 to the heterogeneous class, since in different parts of the domain we have different

118 we obtain

$$119 \quad (2.3) \quad \begin{aligned} \hat{e}_1^n &= \hat{e}_1^n(0, k) e^{\sqrt{k^2 + \tilde{\eta}^2} x} = \hat{e}_1^n(0, k) e^{\lambda(k)x} & \text{in } \Omega_1, \\ \hat{e}_2^n &= \hat{e}_2^n(0, k) e^{-kx} = \hat{e}_2^n(0, k) e^{-\gamma(k)x} & \text{in } \Omega_2, \end{aligned}$$

120 where $\tilde{\eta}^2 = \frac{\eta^2}{\nu_1}$. The transmission conditions in (2.2) allow us to express the Fourier
121 coefficient at iteration n of the solution in one subdomain as function of the coefficient
122 of the solution in the other subdomain at the previous iteration $n - 1$, namely

$$123 \quad (2.4) \quad \hat{e}_1^n(0, k) = \frac{-\nu_2 \gamma(k) + \sigma_1(k)}{\nu_1 \lambda(k) + \sigma_1(k)} \hat{e}_2^{n-1}(0, k),$$

124 and

$$125 \quad (2.5) \quad \hat{e}_2^n(0, k) = \frac{\nu_1 \lambda(k) - \sigma_2(k)}{-\nu_2 \gamma(k) - \sigma_2(k)} \hat{e}_1^{n-1}(0, k).$$

126 Combining (2.4) and (2.5) we get

$$127 \quad \hat{e}_1^n(0, k) = \frac{-\nu_2 \gamma(k) + \sigma_1(k)}{\nu_1 \lambda(k) + \sigma_1(k)} \cdot \frac{\nu_1 \lambda(k) - \sigma_2(k)}{-\nu_2 \gamma(k) - \sigma_2(k)} \hat{e}_1^{n-2}(0, k).$$

128 By induction we then obtain

$$129 \quad \hat{e}_1^{2n}(0, k) = \rho^n \hat{e}_1^0(0, k) \quad \hat{e}_2^{2n}(0, k) = \rho^n \hat{e}_2^0(0, k),$$

130 where the convergence factor ρ is defined by

$$131 \quad \rho := \rho(k, \sigma_1, \sigma_2) = \frac{-\nu_2 \gamma(k) + \sigma_1(k)}{\nu_1 \lambda(k) + \sigma_1(k)} \cdot \frac{\nu_1 \lambda(k) - \sigma_2(k)}{-\nu_2 \gamma(k) - \sigma_2(k)}.$$

132 Expressing the dependence on the Fourier frequency k we get

$$133 \quad (2.6) \quad \rho(k, \sigma_1, \sigma_2) = \frac{-\nu_2 k + \sigma_1(k)}{\nu_1 \sqrt{k^2 + \tilde{\eta}^2} + \sigma_1(k)} \cdot \frac{\nu_1 \sqrt{k^2 + \tilde{\eta}^2} - \sigma_2(k)}{-\nu_2 k - \sigma_2(k)}.$$

134 A closer inspection of (2.6) leads us to conclude that if we chose the operators S_j
135 such that their eigenvalues are

$$136 \quad (2.7) \quad \sigma_1^{\text{opt}}(k) := \nu_2 k \quad \text{and} \quad \sigma_2^{\text{opt}}(k) := \nu_1 \sqrt{k^2 + \tilde{\eta}^2},$$

137 then we would have $\rho \equiv 0$. In this case the algorithm would converge in just two
138 iterations. This option, even though it is optimal, leads to non local operators S_j^{opt} ,
139 which correspond to the Schur complements [29], and they are expensive from the
140 computational point of view. Indeed, the operator associated to the eigenvalues
141 $\sigma_1^{\text{opt}}(k) := \nu_2 k$ corresponds to the square root of the Laplacian on the interface Γ ,
142 i.e. $S_1^{\text{opt}} = \nu_2 (-\Delta_\Gamma)^{\frac{1}{2}}$ which is a fractional and non local operator. The non-local
143 property of S_1^{opt} can also be understood considering a discretization of the straight
144 interface Γ and the discrete counterpart of S_1^{opt} , i.e. $S_{1h}^{\text{opt}} := \nu_2 (-\Delta_{y,h})^{\frac{1}{2}}$ where
145 $-\Delta_{y,h} = \text{diag}(-1, 2, -1)$ is the classical 1-D Laplacian. A direct implementation
146 shows that the matrix S_{1h}^{opt} is dense. Even though the use of S_{1h}^{opt} would destroy the
147 sparsity of the subdomain matrices, theoretically it could still be used as a transmis-
148 sion condition and the method would then converge in two iterations. However, the

149 major drawback is that in general we do not know the operator S_j^{opt} and therefore
 150 we would have to assemble numerically the Schur complements. This is an operation
 151 which requires the knowledge of the inverse of the subdomain operators and therefore
 152 it is computationally expensive.

153 We thus look for classes of convenient transmission conditions which are amenable
 154 to easy implementation, and then to find which transmission conditions among a
 155 specific class lead to the best convergence factor. We consider here zeroth order
 156 approximations of the optimal operators in (2.7) which correspond to classical Robin
 157 conditions on the interface. In order to get the best transmission conditions in terms
 158 of convergence speed, we have to minimize the maximum of the convergence factor
 159 over all the frequencies k . Defining $\mathcal{D}_1, \mathcal{D}_2$ as the classes of transmission conditions,
 160 we are looking for a couple $(\sigma_1^*, \sigma_2^*) \in \mathcal{D} := \mathcal{D}_1 \times \mathcal{D}_2$ such that

161 (2.8)
$$(\sigma_1^*, \sigma_2^*) = \arg \min_{(\sigma_1, \sigma_2) \in \mathcal{D}} \left(\max_{k_{\min} \leq k \leq k_{\max}} |\rho(k, \sigma_1, \sigma_2)| \right).$$

162 The lower and upper bounds k_{\min}, k_{\max} depend on the problem under study: k_{\min}
 163 is given by the Fourier expansion and here it is equal to $k_{\min} = \frac{\pi}{L}$. The presence of
 164 k_{\min} in (2.8), is the “memory” that our problem has of the boundness of the domain,
 165 see [11, 20, 19] for more details on the influence of the domain for optimized Schwarz
 166 methods. The upper bound k_{\max} is instead the maximum frequency that can be
 167 resolved by the grid and it is typically estimated as $k_{\max} = \frac{\pi}{h}$ where h is a measure
 168 of the grid spacing.

169 **2.1. Zeroth order single sided optimized transmission conditions.** Let p
 170 be a free parameter, we define

171 (2.9)
$$\sigma_1(k) = \nu_2 p, \quad \sigma_2(k) = \nu_1 \sqrt{\tilde{\eta}^2 + p^2}.$$

172 We have made this choice because the optimal operators in (2.7) are clearly
 173 rescaled according to the diffusion constants of the two subdomains and thus we
 174 imitate this behaviour. Furthermore we introduce the parameter $\tilde{\eta}^2$ in the definition
 175 of $\sigma_2(k)$ in order to make the problem amenable to analytical treatment. With this
 176 choice, we have $\sigma_j(k) = \sigma_j^{\text{opt}}(k)$ for $k = p$; in other words, for the frequency $k = p$,
 177 the transmission conditions lead to an exact solver which converges in two iterations.
 178 The idea of introducing free parameters such that the eigenvalues $\sigma_j(k)$ are identical
 179 to the optimal ones for a certain frequency is essential, because as we will see in the
 180 following, it allows us to solve the min-max problems which, for a generic choice of
 181 σ_j , are extremely hard to solve.

182 Inserting the expressions (2.9) into (2.6), the min-max problem (2.8) becomes

183 (2.10)
$$\min_{p \in \mathbb{R}} \max_{k_{\min} \leq k \leq k_{\max}} \left| \frac{k - p}{k + \lambda \sqrt{p^2 + \tilde{\eta}^2}} \cdot \frac{\sqrt{k^2 + \tilde{\eta}^2} - \sqrt{p^2 + \tilde{\eta}^2}}{\sqrt{k^2 + \tilde{\eta}^2} + \frac{p}{\lambda}} \right|,$$

184 where $\lambda = \frac{\nu_1}{\nu_2}$. We define $\rho(k, p) := \frac{k - p}{k + \lambda \sqrt{p^2 + \tilde{\eta}^2}} \cdot \frac{\sqrt{k^2 + \tilde{\eta}^2} - \sqrt{p^2 + \tilde{\eta}^2}}{\sqrt{k^2 + \tilde{\eta}^2} + \frac{p}{\lambda}}$. We are now solving

185 the min-max problem (2.10). The main steps are the following:

- 186
 - 187 • Restricting the range in which we are searching for p .
 - 188 • Identifying the candidates for the maxima in the variable k .
 - 189 • Studying how the maxima behave when varying the parameter p .

189 LEMMA 2.1 (Restriction for the interval of p). *If p^* is a solution to problem*
 190 *(2.10) then p^* belongs to the interval $[k_{\min}, k_{\max}]$.*

191 *Proof.* First we note that $|\rho(k, p)| < |\rho(k, -p)|$ for every $p \geq 0$. Therefore we can
 192 assume $p^* \in \mathbb{R}^+$. Moreover the function is always positive and equal to zero only
 193 for $k = p$. Thus we can neglect the absolute value. Direct calculations show that
 194 $\frac{\partial \rho(k, p)}{\partial p} = h(k, p)$ where
 (2.11)

$$195 \quad h(k, p) := \frac{(p-k)\lambda p(\sqrt{k^2 + \bar{\eta}^2}\lambda + k)}{(k + \lambda\sqrt{p^2 + \bar{\eta}^2})^2(\sqrt{k^2 + \bar{\eta}^2}\lambda + p)\sqrt{p^2 + \bar{\eta}^2}} + \frac{(\sqrt{p^2 + \bar{\eta}^2} - \sqrt{k^2 + \bar{\eta}^2})\lambda(\sqrt{k^2 + \bar{\eta}^2}\lambda + k)}{(k + \lambda\sqrt{p^2 + \bar{\eta}^2})(\sqrt{k^2 + \bar{\eta}^2}\lambda + p)^2}.$$

196 We observe that if $p^* < k_{\min}$ then $\frac{\partial \rho}{\partial p}(k, p^*) < 0$ for all $k \in [k_{\min}, k_{\max}]$, hence we are
 197 for sure not at the optimum since increasing p^* would decrease the convergence factor
 198 for all the frequencies $k \in [k_{\min}, k_{\max}]$.

199 On the other hand if $p^* > k_{\max}$ then we have $\frac{\partial \rho}{\partial p}(k, p^*) > 0 \forall k \in [k_{\min}, k_{\max}]$.
 200 Hence we cannot be at the optimum either since decreasing p^* would decrease $\rho(k, p)$
 201 $\forall k \in [k_{\min}, k_{\max}]$. Thus we can conclude that if p^* is a solution of (2.10), then p^* lies
 202 in the interval $[k_{\min}, k_{\max}]$. \square

203 Now we focus on the search of the maxima of $\rho(p, k)$ with respect to k keeping in
 204 mind that p belongs to $[k_{\min}, k_{\max}]$.

205 LEMMA 2.2 (Local maxima in k). *For any fixed value of $p \in [k_{\min}, k_{\max}]$, the*
 206 *function $k \rightarrow \rho(k, p)$ assumes its maximum either at $k = k_{\min}$ or at $k = k_{\max}$.*

207 *Proof.* We consider the derivative of $\rho(k, p)$ with respect to k and we remind that
 208 $\rho(k, p)$ is always positive so we may neglect the absolute value. Direct calculations
 209 show that $\frac{\partial \rho}{\partial k} = h(p, k)$. Thus considering (2.11) we have that letting $p \in (k_{\min}, k_{\max})$,
 210 $\frac{\partial \rho}{\partial k} < 0, \forall k < p$, and $\frac{\partial \rho}{\partial k} > 0, \forall k > p$. Therefore the maximum is attained on the
 211 boundary, either at $k = k_{\min}$ or $k = k_{\max}$.

212 On the other hand, if $p = k_{\min}$, $\rho(k, k_{\min})$ has a zero in $k = k_{\min}$. For all the other
 213 values of k in the interval $[k_{\min}, k_{\max}]$, the function is strictly increasing and therefore
 214 the maximum is attained at $k = k_{\max}$. The case $p = k_{\max}$ is identical and hence the
 215 result follows. \square

216 We now have all the ingredients to solve the min-max problem (2.10).

217 THEOREM 2.3. *The unique optimized Robin parameter p^* solving the min-max*
 218 *problem (2.10) is given by the unique root of the non linear equation*

$$219 \quad (2.12) \quad |\rho(k_{\min}, p^*)| = |\rho(k_{\max}, p^*)|.$$

220 *Proof.* From the previous lemmas, we know that we can rewrite problem (2.10)
 221 as

$$222 \quad \min_{p \in [k_{\min}, k_{\max}]} \max \{ \rho(k_{\min}, p), \rho(k_{\max}, p) \},$$

223 i.e. the maximum is either attained at $k = k_{\min}$ or $k = k_{\max}$. We now show that the
 224 optimal p^* satisfies a classical equioscillation property [32], see Fig 2 for a graphical
 225 representation. We first note that $\rho(k_{\min}, p) = 0$ for $p = k_{\min}$, and $\frac{\partial \rho(k_{\min}, p)}{\partial p} > 0, \forall p \in$
 226 (k_{\min}, k_{\max}) . Therefore increasing p , $\rho(k_{\min}, p)$ strictly increases until it reaches its
 227 maximum value for $p = k_{\max}$. On the other hand, we have that $\rho(k_{\max}, k_{\min})$ is strictly
 228 greater than zero, and while p increases from k_{\min} to k_{\max} , $\rho(k_{\max}, p)$ decreases, being
 229 $\frac{\partial \rho(k_{\max}, p)}{\partial p} < 0, \forall p \in [k_{\min}, k_{\max})$. Furthermore we have that $\rho(k_{\max}, k_{\max}) = 0$.

230 Hence, thanks to the strict monotonicity of both $\rho(k_{\min}, p)$ and $\rho(k_{\max}, p)$, there
 231 exists by continuity a unique value p^* such that $\rho(k_{\min}, p^*) = \rho(k_{\max}, p^*)$. This value
 232 is clearly the optimum, because perturbing p^* would increase the value of ρ at one of
 233 the two extrema and therefore the maximum of ρ over all k . \square

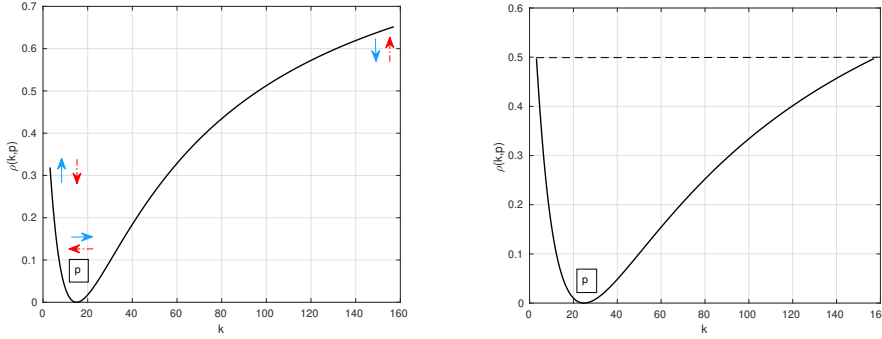


Fig. 2: Illustration of the equioscillation property described in Theorem 2.3.

234 Even though a closed form solution of (2.12) is not known, it is interesting to study
 235 asymptotically how the algorithm performs. Therefore we keep ν_1, ν_2 and $\tilde{\eta}^2$ fixed,
 236 and $k_{\max} = \frac{\pi}{h}$ while letting $h \rightarrow 0$. This is a case of interest since usually we want
 237 to decrease the mesh size h in order to get a better approximation and therefore it
 238 is useful to see how the method performs in this regime. We introduce the notation
 239 $f(h) \sim g(h)$ as $h \rightarrow 0$ if and only if $\lim_{h \rightarrow 0} \frac{f(h)}{g(h)} = 1$.

240 **THEOREM 2.4.** Let $D := \sqrt{k_{\min}^2 + \tilde{\eta}^2}$. Then if $\nu_1, \nu_2, \tilde{\eta}^2$ are kept fixed, $k_{\max} = \frac{\pi}{h}$
 241 and h is small enough, then the optimized Robin parameter p^* is given by

$$242 \quad (2.13) \quad p^* \sim C \cdot h^{-\frac{1}{2}}, \quad C := \sqrt{\frac{(\lambda D + k_{\min})\pi}{(\lambda + 1)}}.$$

243 Furthermore the asymptotic convergence factor of the heterogeneous optimized Schwarz
 244 method is

$$245 \quad (2.14) \quad \max_{k_{\min} \leq k \leq \pi/h} |\rho(k, p^*)| \sim 1 - h^{\frac{1}{2}} \left[\frac{\lambda D}{C} + \frac{D}{C} + \frac{k_{\min}}{\lambda C} + \frac{k_{\min}}{C} \right].$$

246 *Proof.* We make the ansatz $p = C \cdot h^{-\alpha}$ in the equation (2.12). Expanding for
 247 small h , we get that

$$248 \quad |\rho(k_{\min}, p)| \sim 1 - h^\alpha \left[\frac{\lambda D}{C} + \frac{D}{C} + \frac{k_{\min}}{\lambda C} + \frac{k_{\min}}{C} \right].$$

249 On the other hand,

$$250 \quad |\rho(k_{\max}, p)| \sim 1 - h^{1-\alpha} \left[\frac{\lambda C}{\pi} + \frac{2C}{\pi} + \frac{C}{\lambda \pi} \right].$$

251 Comparing the first two terms we get the result. \square

252 *Remark 2.5.* Note that if we set $\tilde{\eta}^2 = 0$, then we recover the results for the
 253 coupling of two Laplace equations with different diffusion constants, see [12]. In that
 254 case,

$$255 \quad \rho \sim 1 - h^{\frac{1}{2}} \sqrt{\frac{k_{\min}}{\pi}} \left[\frac{(\lambda + 1)^2}{\lambda} \right], \quad p^* = \sqrt{k_{\min} \pi} h^{-\frac{1}{2}}.$$

$\tilde{\eta}$	p^*	\bar{p}	$\max_k \rho(k, p^*)$	$\max_k \rho(k, \bar{p})$
1	22.47	22.47	0.5618	0.5618
100	72.11	110.09	0.0737	0.0452
500	92.21	508.2691	0.0025	0.0081
1000	95	1005	$3.74 \cdot 10^{-4}$	0.0026

Table 1: Comparison between the optimal solution p^* of Theorem 2.3 and the optimal solution \bar{p} computed numerically for the min-max problem involving $\sigma_1(k) = \nu_2 p$ and $\sigma_2(k) = \nu_1 p$. Mesh size equal to $h = \frac{1}{50}$.

Moreover we have that the convergence factor (2.14) satisfies for $\lambda = \frac{\nu_1}{\nu_2} \rightarrow \infty$, $|\rho| \sim 1 - h^{\frac{1}{2}} \lambda \sqrt{\frac{D}{\pi}}$ and for $\lambda \rightarrow 0$, $|\rho| \sim 1 - h^{\frac{1}{2}} \frac{1}{\lambda} \sqrt{\frac{k_{\min}}{\pi}}$. On the other hand as $\tilde{\eta} \rightarrow \infty$ we have $|\rho| \sim 1 - h^{\frac{1}{2}} \sqrt{\tilde{\eta}} \frac{(\lambda+1)^{\frac{3}{2}}}{\sqrt{\lambda\pi}}$. It follows that for all strong heterogeneity limits, the constant in front of the asymptotic term $h^{\frac{1}{2}}$ becomes larger, therefore the deterioration is slower and the method is more efficient.

Remark 2.6. One could object that if we set $\sigma_1(k) = \nu_2 p$ and $\sigma_2(k) = \nu_1 p$, without introducing the ad-hoc term involving $\tilde{\eta}$ in the definition $\sigma_2(k)$, it may be possible to improve the method. In this case the convergence factor would have two zeros, one located at $k_1 := p$ and the other one located in $k_2 := \sqrt{p^2 - \tilde{\eta}^2}$. The min-max problem is then much harder to solve analytically because one of the zeros depends on the parameter p in a non-linear way. Furthermore for $p < \tilde{\eta}$ the second zero is not real, for values of p slightly larger than $\tilde{\eta}$, the distance between the two zeros might be significant while if p is very large then $k_1 \approx k_2$. A large number of different cases arises which make the min-max problem really hard to solve. However, even though we are unable to solve the min-max problem for a general setting of parameters, it is possible to draw conclusions in the case in which k_{\max} is large enough. In fact from an analysis of the convergence factor we deduce that $\rho(k_{\max}, p) \rightarrow 1$ as $h \rightarrow 0$. If we impose equioscillation between $\rho(k_{\min}, p)$ and $\rho(k_{\max}, p)$, calculations show that then p goes to infinity as $h \rightarrow 0$ and therefore we have three local maxima in the interval $[k_{\min}, k_{\max}]$, two at the boundary and an interior maximum, \hat{k} located between the two zeros. Estimating asymptotically $|\rho(\hat{k}, p)|$ as $h \rightarrow 0$ using the convexity of the function in the interval $[k_1, k_2]$ we obtain

$$|\rho(\hat{k}, p)| \leq \frac{\partial \rho}{\partial k} \Big|_{(k=\sqrt{p^2 - \tilde{\eta}^2}, p)} \cdot |p - \sqrt{p^2 - \tilde{\eta}^2}| \approx h^2 + o(h^2).$$

Then observing instead that the value of ρ tends to one at the boundaries, it follows that the optimal solution is indeed obtained by equioscillations between the extreme points and the interior point does not play a role. Repeating the analogous calculations of Theorem 2.4, we find that p has the same asymptotic expression as in the previous theorem. We can then conclude that, for $h \rightarrow 0$, the two min-max problems with different $\sigma_2(k)$ lead to equivalent optimized parameters. In the non asymptotic regime, Table 1 shows that the two choices are equivalent for moderate values of $\tilde{\eta}$. For very large values of $\tilde{\eta}$, then (2.9) leads to a more efficient method.

2.2. Zeroth order two sided optimized transmission conditions. Let us consider now the more general case for Robin transmission conditions, with two free

289 parameters p and q such that the operators S_j have eigenvalues

$$290 \quad \sigma_1(k) = \nu_2 p, \quad \sigma_2(k) = \nu_1 \sqrt{q^2 + \tilde{\eta}^2}.$$

291 We remark that, according to this choice, $\sigma_1(k)$ is exact for the frequency $k = p$
 292 while $\sigma_2(k)$ is exact for frequency $k = q$. Therefore from (2.6) we deduce the method
 293 converges in two iterations for two frequencies. Letting again $\lambda = \frac{\nu_1}{\nu_2}$, we get
 (2.15)

$$294 \quad \min_{p,q} \max_{k_{\min} \leq k \leq k_{\max}} |\rho(k, p, q)| = \min_{p,q} \max_{k_{\min} \leq k \leq k_{\max}} \left| \frac{(k-p)(\sqrt{k^2 + \tilde{\eta}^2} - \sqrt{q^2 + \tilde{\eta}^2})}{(k + \lambda\sqrt{q^2 + \tilde{\eta}^2})(\sqrt{k^2 + \tilde{\eta}^2} + \frac{p}{\lambda})} \right|.$$

295 Following the same philosophy of the previous section, we start restricting the range
 296 in which we need to search for the parameters p and q . Then we focus on the maxima
 297 with respect to k and finally we analyse how these maxima behave with respect to p
 298 and q .

299 **LEMMA 2.7** (Restriction for the interval of p, q). *If the couple (p^*, q^*) is a solution*
 300 *to the min-max problem (2.15), then we have that both p^* and q^* belong to the interval*
 301 *$[k_{\min}, k_{\max}]$.*

302 *Proof.* For $p > 0$, we observe that $|\rho(k, p, q)| < |\rho(k, -p, q)|$ and q is always
 303 squared so we can restrict both parameters to be positive without loss of generality.
 304 Next we consider the partial derivatives of $|\rho|$ with respect to p and q :

$$305 \quad (2.16) \quad \text{sign} \left(\frac{\partial |\rho|}{\partial p} \right) = -\text{sign}(k - p), \quad \text{sign} \left(\frac{\partial |\rho|}{\partial q} \right) = -\text{sign}(k - q).$$

306 Repeating the same argument of Lemma 2.1, we conclude that we are not at the
 307 optimum unless both p and q belong to $[k_{\min}, k_{\max}]$. \square

308 Next we analyse the behaviour of $|\rho(k, p, q)|$ with respect to the variable k , trying to
 309 identify the local maxima.

310 **LEMMA 2.8** (Local maxima in k). *For $p, q \in [k_{\min}, k_{\max}]$,*

$$311 \quad \max_{k_{\min} \leq k \leq k_{\max}} |\rho(k, p, q)| = \max\{|\rho(k_{\min}, p, q)|, |\rho(\hat{k}, p, q)|, |\rho(k_{\max}, p, q)|\},$$

312 *where \hat{k} is an interior maximum always between $[\min(p, q), \max(p, q)]$.*

313 *Proof.* We first observe that $|\rho(k, p, q)|$ has two zeros, one at $k = p$ and the other
 314 at $k = q$. Next we consider the derivative of $\rho(k, p, q)$ with respect to k and assuming
 315 that $p \neq q$ ¹ we get,

$$316 \quad (2.17) \quad \frac{\partial \rho(k, p, q)}{\partial k} = \frac{(\sqrt{k^2 + \tilde{\eta}^2} - \sqrt{q^2 + \tilde{\eta}^2})(\sqrt{k^2 + \tilde{\eta}^2})(\sqrt{k^2 + \tilde{\eta}^2} + \frac{p}{\lambda})(\lambda\sqrt{q^2 + \tilde{\eta}^2} + p)}{D(k, p)} +$$

$$+ \frac{(k-p)(k + \lambda\sqrt{q^2 + \tilde{\eta}^2})k(\frac{p}{\lambda} + \sqrt{q^2 + \tilde{\eta}^2})}{D(k, p)}.$$

317 The denominator $D(k, p)$ is always positive. Now we consider the two cases in which
 318 $k < \min(p, q)$ and $k > \max(p, q)$: in both we have that $\rho(k, p, q) > 0$, and analyzing
 319 equation (2.17) we conclude that for $k < \min(p, q)$, $\frac{\partial \rho(k, p)}{\partial k} < 0$ and for $k > \max(p, q)$,

¹If $p = q$ we are considering the optimization problem discussed in the previous paragraph.

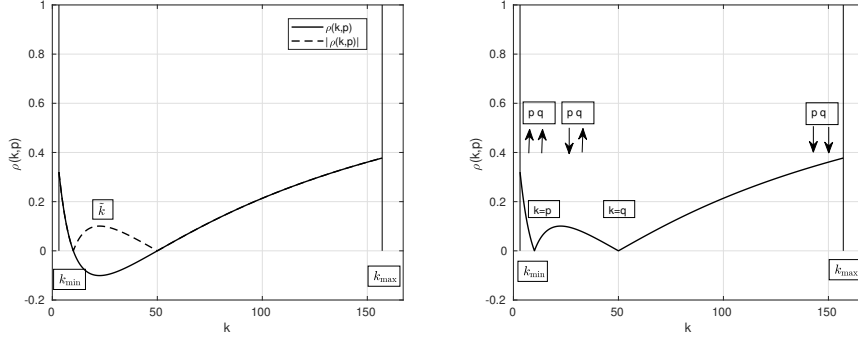


Fig. 3: The left panel shows an example of the convergence factor with its three local maxima localized at $k = k_{\min}$, $k = k_{\max}$ and $k = \hat{k}$. On the right we summarize how these local maxima behave as function of p and q .

320 $\frac{\partial \rho}{\partial k} > 0$. Hence by continuity of $\partial_k \rho(k, p)$, there exists at least one \hat{k} , which is a local
 321 minimum of $\rho(k, p)$ and a local maximum for $|\rho(k, p)|$ see Fig. 3, such that $\partial_k \rho = 0$,
 322 and all of them lie in the interval $[\min(p, q), \max(p, q)]$ for p and q fixed. Now we
 323 prove that the interior maximum is unique. Indeed the interior maxima for $|\rho(k, p, q)|$
 324 are given by the roots of the equation $\partial_k \rho(k, p) = 0$ which corresponds to

$$325 \quad (2.18) \quad \frac{\sqrt{q^2 + \tilde{\eta}^2} - \sqrt{\tilde{\eta}^2 + k^2}}{k + \lambda \sqrt{\tilde{\eta}^2 + q^2}} = \frac{(k - p)k}{(\lambda \sqrt{k^2 + \tilde{\eta}^2} + p) \sqrt{k^2 + \tilde{\eta}^2}}.$$

326 First we suppose that $p < k < q$. Then we have that the left hand side of (2.18) is
 327 positive in $k = p$, it is strictly decreasing in k , and it reaches zero at $k = q$. The
 328 right hand side of (2.18) instead starts from zero and it is strictly increasing. We
 329 conclude that there is a unique point \hat{k} such that the two sides are equal and hence
 330 a unique interior maximum \hat{k} for $|\rho(k, p, q)|$. If instead $q < k < p$, changing the sign
 331 of (2.18) and dividing by $k/\sqrt{k^2 + \tilde{\eta}^2}$, the right hand side is strictly decreasing while
 332 the left hand side, computing the derivative, is strictly increasing and hence the same
 333 conclusion holds.

334 We may conclude that the function assumes its maximum either at the interior point
 335 \hat{k} , or at the boundaries of the interval, i.e. k_{\min} , k_{\max} . \square

336 In the next lemma we prove that the end points k_{\min} and k_{\max} satisfy an equioscillation
 337 property as in the previous case of a single parameter p .

338 **LEMMA 2.9** (Equioscillation at the end points). *The optimized convergence fac-*
 339 *tor $|\rho(k, p, q)|$ must satisfy equioscillation at the endpoints, i.e.*

$$340 \quad |\rho(k_{\min}, p^*, q^*)| = |\rho(k_{\max}, p^*, q^*)|.$$

341 *Proof.* We study how $|\rho(k_{\min}, p, q)|$, $|\rho(\hat{k}, p, q)|$ and $|\rho(k_{\max}, p, q)|$ behave as p, q
 342 vary and we show that if we do not have equioscillation at the boundary points, we
 343 can always improve the convergence factor until equioscillation is reached. Taking
 344 into account (2.16) we have for every $p, q \in [k_{\min}, k_{\max}]$

$$345 \quad \frac{\partial |\rho(k_{\min}, p, q)|}{\partial p} > 0, \quad \frac{\partial |\rho(k_{\min}, p, q)|}{\partial q} > 0,$$

346

347

$$\frac{\partial|\rho(k_{\max}, p, q)|}{\partial p} < 0, \quad \frac{\partial|\rho(k_{\max}, p, q)|}{\partial q} < 0.$$

348

349

350

351

352

In other words, increasing independently p, q increases $|\rho(k_{\min}, p, q)|$ and decreases $|\rho(k_{\max}, p, q)|$. We now compute the total derivative of $|\rho(\tilde{k}, p, q)|$ with respect to p and q , which since we have $\partial_k|\rho(\tilde{k}, p, q)| = 0$, corresponds to the partial derivative with respect to the two arguments. One then finds that the sign of $\frac{\partial|\rho(\tilde{k}, p, q)|}{\partial p}$ and $\frac{\partial|\rho(\tilde{k}, p, q)|}{\partial q}$ depends on the position of \tilde{k} with respect to p and q . Indeed it holds

353

$$\text{sign}\left(\frac{\partial|\rho(\tilde{k}, p, q)|}{\partial p}\right) = \text{sign}(p - \tilde{k}), \quad \text{sign}\left(\frac{\partial|\rho(\tilde{k}, p, q)|}{\partial q}\right) = \text{sign}(q - \tilde{k}).$$

354

355

356

357

358

359

360

361

362

363

364

365

366

367

368

369

370

371

The right panel of Fig. 3 summarizes the dependence of the local maxima with respect to p and q . Let us suppose that $p < q$, q fixed, and $|\rho(k_{\min}, p, q)| < |\rho(k_{\max}, p, q)|$. The other cases are treated similarly. We do not make any assumptions on the value of $|\rho(\tilde{k}, p, q)|$. Now if we increase p we decrease $\max\{|\rho(k_{\min}, p, q)|, |\rho(\tilde{k}, p, q)|, |\rho(k_{\max}, p, q)|\}$ as long as $|\rho(k_{\min}, p, q)| \leq |\rho(k_{\max}, p, q)|$ and $p \leq q$. If $|\rho(k_{\min}, p, q)| = |\rho(k_{\max}, p, q)|$ for a certain $p < q$, then we obtain the desired result since we have improved uniformly the convergence factor. Suppose instead that when $p = q$, and therefore $|\rho(\tilde{k}, p, q)| = 0$, we still have $|\rho(k_{\min}, p, q)| < |\rho(k_{\max}, p, q)|$. Thus the convergence factor is equal to $|\rho(k_{\max}, p, q)|$. We now set up a process which improves $\max_{[k_{\min}, k_{\max}]} |\rho(k, p, q)|$ until we get equioscillation at the boundary points. As long as $|\rho(k_{\min}, p, q)| < |\rho(k_{\max}, p, q)|$, we increase $p > q$ until $|\rho(\tilde{k}, p, q)| \leq |\rho(k_{\max}, p, q)|$. When we reach $|\rho(\tilde{k}, p, q)| = |\rho(k_{\max}, p, q)|$, we then increase q until $q = p$. If while increasing q we still have $|\rho(k_{\min}, p, q)| < |\rho(k_{\max}, p, q)|$, then we repeat the process. Continuing this process, we must reach equioscillation at some point by continuity since when p approaches k_{\max} , we must have $|\rho(k_{\min}, k_{\max}, q)| > |\rho(k_{\max}, k_{\max}, q)| = 0$. At the same time we improved surely the convergence factor since, in spite of the initial value of $|\rho(\tilde{k}, p, q)|$, we have that $\max_{[k_{\min}, k_{\max}]} |\rho(k, p, q)| \leq |\rho(k_{\max}, p, q)|$ which is decreasing along the process. \square

372

We now have enough tools and insights to prove the main results of this section:

373

374

THEOREM 2.10. *There are two pairs of parameters (p_1^*, q_1^*) and (p_2^*, q_2^*) such that we obtain equioscillation between all the three local maxima,*

375

$$(2.19) \quad |\rho(k_{\min}, p_j^*, q_j^*)| = |\rho(k_{\max}, p_j^*, q_j^*)| = |\rho(\hat{k}, p_j^*, q_j^*)| \quad j = 1, 2.$$

376

The optimal pair of parameters is the one which realizes the

377

$$(2.20) \quad \min_{(p_j^*, q_j^*), j=1,2} |\rho(k_{\min}, p_j^*, q_j^*)|.$$

Proof. Let us define $F_1(p, q) := \rho(k_{\min}, p, q)$ and $F_2(p, q) := \rho(k_{\max}, p, q)$. Due to Lemma 2.9, we know that there exist values (p, q) such that $F := |F_1(p, q)| - |F_2(p, q)| = 0$. We can thus express one parameter, for example q , as a function of the other one, i.e. $q = q(p)$. Although the expression is too complicated to be used for analytical computations, we are able to infer about the structure of $q(p)$. First of all we can state that $q(p = k_{\min}) = k_{\max}$ since $|F_1(k_{\min}, q(k_{\min}))| = 0$ implies that $|F_2(k_{\min}, q(k_{\min}))| = 0$ but then the only choice possible is $q(k_{\min}) = k_{\max}$. Similarly we have $q(k_{\max}) = k_{\min}$. We next use implicit differentiation to infer about the

behaviour of q with respect to p .

Following classical arguments we have that, since $F(p, q(p)) = 0$,

$$0 = \frac{dF(p, q(p))}{dp} = \frac{dF_1(p, q(p)) - dF_2(p, q(p))}{dp} = \frac{\partial F_1 - \partial F_2}{\partial p} + \frac{\partial F_1 - \partial F_2}{\partial q} q'(p),$$

378 and therefore

$$379 \quad (2.21) \quad q'(p) = \frac{\frac{\partial F_2}{\partial p} - \frac{\partial F_1}{\partial p}}{\frac{\partial F_1}{\partial q} - \frac{\partial F_2}{\partial q}}.$$

380 Analyzing carefully the sign of each term, we conclude that $q'(p) < 0 \quad \forall p \in (k_{\min}, k_{\max})$. ■

381 Therefore we state that $q(p)$ is a strictly decreasing function which starts from $q(p =$

382 $k_{\min}) = k_{\max}$ and reaches its minimum at $q(k_{\max}) = k_{\min}$.

383 Now we have only one free parameter p , since q is constrained to vary such that the

384 equioscillation between the ends points is achieved, thus we look for values of p such

385 that we obtain equioscillation between k_{\min} and the interior maximum \hat{k} .

386 Let us first study how $\tilde{F}(p, q) := \rho(\hat{k}, p, q(p))$ behaves while p varies. As long as

387 $p \leq \hat{k} \leq q(p)$, we have

$$388 \quad \text{sign} \left(\frac{\partial |\tilde{F}(p, q(p))|}{\partial p} \right) = \text{sign}(\sqrt{q(p)^2 + \tilde{\eta}^2} - \sqrt{\hat{k}^2 + \tilde{\eta}^2}) \cdot \text{sign}(\tilde{F}(p, q(p))) < 0,$$

$$389 \quad \text{sign} \left(\frac{\partial |\tilde{F}(p, q(p))|}{\partial q} \right) = \text{sign}(p - \hat{k}) \cdot \text{sign}(\tilde{F}(p, q(p))) > 0.$$

390

391 Then, keeping in mind the $q'(p) < 0$, $\tilde{F}(p, q(p))$ is strictly decreasing for all the values

392 of p such that $p < \hat{k} < q(p)$,

$$393 \quad \frac{d|\tilde{F}(p, q(p))|}{dp} = \frac{\partial |\tilde{F}(p, q(p))|}{\partial p} + \frac{\partial |\tilde{F}(p, q(p))|}{\partial q} \cdot q'(p) < 0.$$

394 Similarly it is straightforward to verify that for $q(p) < \hat{k} < p$

$$395 \quad \frac{d|\tilde{F}(p, q(p))|}{dp} = \frac{\partial |\tilde{F}(p, q(p))|}{\partial p} + \frac{\partial |\tilde{F}(p, q(p))|}{\partial q} \cdot q'(p) > 0.$$

396 Moreover we have that for $p = \hat{k} = q(p)$, $|\tilde{F}(p, q(p))| = 0$ and $\frac{d|\tilde{F}(p, q(p))|}{dp} = 0$.

397 Focusing next on $|F_1(p, q(p))|$ we can state that, neglecting the $\text{sign}(F_1(p, q(p)))$, be-

398 cause it is always positive or zero, the derivatives at the left and right boundary

399 extrema are equal to

$$400 \quad \frac{d|F_1(k_{\min}, k_{\max})|}{dp} = \frac{\partial |F_1(k_{\min}, k_{\max})|}{\partial p} + \frac{\partial |F_1(k_{\min}, k_{\max})|}{\partial q} q'(p) = \frac{\partial |F_1(k_{\min}, k_{\max})|}{\partial p} > 0, \blacksquare$$

401 and

$$402 \quad \frac{d|F_1(k_{\max}, k_{\min})|}{dp} = \frac{\partial |F_1(k_{\max}, k_{\min})|}{\partial p} + \frac{\partial |F_1(k_{\max}, k_{\min})|}{\partial q} q'(p) = \frac{\partial |F_1(k_{\max}, k_{\min})|}{\partial p} < 0. \blacksquare$$

403 So for values of p in a right neighbourhood of $p = k_{\min}$, $|F_1(p, q(p))|$ increases, while

404 for values of p in a left neighbourhood of $p = k_{\max}$, $|F_1(p, q(p))|$ decreases. Using the

405 monotonicity of $|F(\hat{k}, p, q(p))|$ and the fact that when $\hat{k} = p = q(p)$, $|F(\hat{k}, p, q(p))| = 0$,
 406 while $|F(k_{\min}, p, q(p))| > 0$, we conclude that there exists at least one pair (p, q) such
 407 that $|F(k_{\min}, p, q(p))| = |F(\hat{k}, p, q(p))|$.

408 We still have to prove that actually there exist only two couples (p_j, q_j) such that
 409 equioscillation is achieved. Indeed, if we imagine that $|F_1(p, q(p))|$ had a certain
 410 behaviour, for example it oscillates, then we might have more than two pairs. Nev-
 411 ertheless we show that $|F_1(p, q(p))|$ has a unique local maximum for $p \in [k_{\min}, k_{\max}]$
 412 so that only two equioscillations are allowed among all the three local maxima: one
 413 while $|\tilde{F}(p, q(p))|$ decreases, the other one for increasing $|\tilde{F}(p, q(p))|$.

414 To do so, we consider $\frac{d|F_1(p, q(p))|}{dp}$ again and substitute (2.21),

$$415 \quad \frac{d|F_1(p, q(p))|}{dp} = \frac{\frac{\partial F_1}{\partial q} \cdot \frac{\partial F_2}{\partial p} - \frac{\partial F_2}{\partial q} \cdot \frac{\partial F_1}{\partial p}}{\frac{\partial F_1}{\partial q} \cdot \frac{\partial F_2}{\partial q}}.$$

416 The zeros of the derivative are given by the non linear equation

$$417 \quad (p - k_{\min})(\sqrt{k_{\max}^2 + \tilde{\eta}^2} - \sqrt{k_{\min}^2 + \tilde{\eta}^2}) \frac{\sqrt{k_{\min}^2 + \tilde{\eta}^2 + \frac{p}{\lambda}}}{\sqrt{k_{\max}^2 + \tilde{\eta}^2 + \frac{p}{\lambda}}} =$$

$$418 \quad (k_{\max} - p)(\sqrt{q^2 + \tilde{\eta}^2} - \sqrt{k_{\min}^2 + \tilde{\eta}^2}) \frac{k_{\min} + \lambda\sqrt{q^2 + \tilde{\eta}^2}}{k_{\max} + \lambda\sqrt{q^2 + \tilde{\eta}^2}}.$$

419

420 It is sufficient to observe that the left hand side starts from 0 and it is strictly increasing
 421 in p , while the right hand side starts from a positive value, it decreases with p and
 422 it reaches 0 for $p = k_{\max}$. So the equation admits only one solution and therefore
 423 the local maximum with respect to p of $|F_1(p, q(p))|$ is unique. The solution to the
 424 min-max problem (2.15) is the pair of parameters (p^*, q^*) which allows equioscillation
 425 among the three local maxima and realizes (2.20). Every other pair of parameter
 426 would led to the increase of at least one of the local maxima and therefore of the
 427 maximum of $|\rho|$ over k . \square

428 In [12], the authors proved a similar result for the Laplace equation with discon-
 429 tinuous coefficients without the presence of the further optimality condition (2.20).
 430 Their result was based on the possibility to restrict the interval of interest for the pa-
 431 rameters to $p < q$ or $q < p$ according to the value of λ . In the present case this is not
 432 possible because of the presence of $\tilde{\eta}^2$ which breaks the symmetry of the convergence
 433 factor. Therefore we cannot discard a priori one of the two possible equioscillations
 434 and the further condition (2.20) must be added. Nevertheless in the asymptotic regime
 435 for $h \rightarrow 0$ and $k_{\max} \rightarrow \infty$, the next result allows us to clearly choose the optimal pair
 436 as a function of λ , recovering the property of the results for the simplified situation
 437 treated in [12].

438 **THEOREM 2.11.** *Let $D := \sqrt{k_{\min}^2 + \tilde{\eta}^2}$. Then if the physical parameters $\tilde{\eta}^2, \nu_1, \nu_2$
 439 are fixed, $k_{\max} = \frac{\pi}{h}$ and h goes to zero, the optimized two-sided Robin parameters are
 440 for $\lambda \geq 1$,*

$$441 \quad (2.22) \quad \begin{aligned} p_1^* &\sim \frac{\lambda(k_{\min} + D)}{\lambda - 1} - \frac{2\sqrt{2}(1 + \lambda)(\lambda D + k_{\min})\lambda^2 \sqrt{\pi(k_{\min} + D)}}{\pi\lambda(\lambda - 1)^3} h^{\frac{1}{2}}, \\ q_1^* &\sim \frac{\pi(\lambda - 1)}{2\lambda} h^{-1} + \frac{\sqrt{2}(1 + \lambda)^2 \sqrt{\pi(k_{\min} + D)}}{2\lambda(\lambda - 1)} h^{-\frac{1}{2}}, \\ \max_{k_{\min} \leq k \leq \pi/h} |\rho(k, p_1^*, q_1^*)| &\sim \frac{1}{\lambda} - \frac{2\sqrt{2}(1 + \lambda)\sqrt{(k_{\min} + D)}}{\sqrt{\pi}\lambda(\lambda - 1)} h^{\frac{1}{2}}, \end{aligned}$$

442 and for $\lambda < 1$ we have

$$\begin{aligned}
443 \quad (2.23) \quad & p_2^* \sim \frac{1}{2}\pi(1-\lambda)h^{-1} + \frac{\sqrt{2}(1+\lambda)^2\sqrt{\pi(D+k_{\min})}}{2(1-\lambda)}h^{-\frac{1}{2}}, \\
& q_2^* \sim \sqrt{\left(\frac{D+k_{\min}}{1-\lambda}\right)^2 - \tilde{\eta}^2} - \frac{2\sqrt{2}(D+k_{\min})^2(\lambda+1)(\lambda D+k_{\min})}{(\lambda-1)^4\sqrt{\pi(D+k_{\min})}\sqrt{\frac{D+k_{\min}}{1-\lambda}-\tilde{\eta}^2}}h^{\frac{1}{2}}, \\
& \max_{k_{\min} \leq k \leq \pi/h} |\rho(k, p_2^*, q_2^*)| \sim \lambda - \frac{2\sqrt{2}\lambda(1+\lambda)\sqrt{(k_{\min}+D)}}{\sqrt{\pi}(1-\lambda)}h^{\frac{1}{2}}.
\end{aligned}$$

444 *Proof.* Guided by numerical experiments, for $\lambda \geq 1$ we make the ansatz $p \sim$
445 $C_p + Ah^{\frac{1}{2}}$, $q \sim Qh^{-1} + Bh^{-\frac{1}{2}}$, and $\hat{k} = C_k h^{-\frac{1}{2}}$. First of all considering the equation
446 $\partial_k \rho(\hat{k}, p, q) = 0$, we find setting to zero the first non zero term $C_k = \sqrt{C_p \cdot Q}$. Insert-
447 ing this into (2.19) and comparing the two leading terms, we get the result. Similarly
448 for $\lambda < 1$, we make the ansatz $p \sim C_p h^{-1} + Ah^{-\frac{1}{2}}$, $q \sim Q + Bh^{\frac{1}{2}}$ and $\hat{k} = C_k h^{-\frac{1}{2}}$ and
449 we get $C_k = \sqrt{C_p \sqrt{Q^2 + \tilde{\eta}^2}}$. Substituting and matching the leading order terms we
450 obtain the result. \square

451 If we set $\tilde{\eta}^2 = 0$, then $D = k_{\min}$ and we recover the results of [12]. Note that in
452 contrast to the one sided case, the convergence factor does not deteriorate to 1 as
453 $h \rightarrow 0$, but it is bounded either by $\frac{1}{\lambda}$ if $\lambda \geq 1$ or by λ if $\lambda < 1$, so we obtain a non-
454 overlapping optimized Schwarz method that converges independently of the mesh size
455 h . We emphasize that the heterogeneity makes the method faster instead of presenting
456 a difficulty. A heuristic explanation is that the heterogeneity tends to decouple the
457 problems, making them less dependent one from the other. In contrast with other
458 domain decomposition methods, optimized Schwarz methods can be tuned according
459 to the physics and therefore they can benefit from this decoupling.

460 **3. Advection Reaction Diffusion-Reaction Diffusion coupling.** In this
461 section, we consider again a domain Ω divided into two subdomains, Ω_1, Ω_2 according
462 to the description at the beginning of Section 2. In Ω_1 we have a reaction diffusion
463 equation, while in Ω_2 we have an advection reaction diffusion equation. We allow
464 the reaction and diffusion coefficients to be different among the subdomains. The
465 optimized Schwarz method reads

$$\begin{aligned}
466 \quad (3.1) \quad & (\eta_1^2 - \nu_1 \Delta) u_1^n = f, \quad \text{in } \Omega_1, \\
& (\nu_1 \partial_x + S_1)(u_1^n)(0, \cdot) = (\nu_2 \partial_x - \mathbf{a} \cdot (1, 0)^\top + S_1)(u_2^{n-1})(0, \cdot), \\
& (\eta_2^2 + \mathbf{a} \cdot \nabla - \nu_2 \Delta) u_2^n = f, \quad \text{in } \Omega_2, \\
& (\nu_2 \partial_x - \mathbf{a} \cdot (1, 0)^\top - S_2)(u_2^n)(0, \cdot) = (\nu_1 \partial_x - S_2)(u_1^{n-1})(0, \cdot),
\end{aligned}$$

467 where $\mathbf{a} = (a_1, a_2)^\top$. The additional term in the transmission conditions arises from
468 the conservation of the flux in divergence form, see Chapter 6 in [31]. We first suppose
469 $a_2 = 0$. Then we can solve the error equations in the subdomains through separation
470 of variables and we obtain $e_i^n = \sum_{k \in \mathcal{V}} \hat{e}_i^n \sin(ky)$, $i = 1, 2$, where

$$471 \quad \hat{e}_1^n(k, x) = A^n(k) e^{\sqrt{\frac{\eta_1^2}{\nu_1} + k^2} x} \quad \hat{e}_2^n(k, x) = B^n(k) e^{\lambda - (k)x},$$

472 and $\lambda_-(k) := \frac{a_1 - \sqrt{a_1^2 + 4\nu_2^2 k^2 + 4\nu_2 \eta_2^2}}{2\nu_2}$. Inserting e_1, e_2 into the transmission conditions
 473 we get

$$474 \quad \nu_1 \sqrt{\frac{\eta_1^2}{\nu_1} + k^2} A^n(k) + \sigma_1(k) A^n(k) = \nu_2 \lambda_-(k) B^{n-1}(k) - a_1 B^{n-1}(k) + \sigma_1(k) B^{n-1}(k),$$

$$\nu_2 \lambda_-(k) B^n(k) - a_1 B^n(k) - \sigma_2(k) B^n(k) = \nu_1 \sqrt{\frac{\eta_1^2}{\nu_1} + k^2} A^{n-1}(k) - \sigma_2(k) A^{n-1}(k).$$

475 The convergence factor is therefore given by

$$476 \quad \rho(k, \sigma_1, \sigma_2) = \frac{\nu_2 \lambda_-(k) - a_1 + \sigma_1(k)}{\nu_1 \sqrt{\tilde{\eta}_1^2 + k^2} + \sigma_1(k)} \frac{\nu_1 \sqrt{\tilde{\eta}_1^2 + k^2} - \sigma_2(k)}{\nu_2 \lambda_-(k) - a_1 - \sigma_2(k)},$$

477 where $\tilde{\eta}_1^2 = \frac{\eta_1^2}{\nu_1}$. We rewrite $\lambda_-(k)$ as $\lambda_-(k) = \frac{a_1}{2\nu_2} - \sqrt{k^2 + \delta^2}$ with $\delta^2 = \frac{a_1^2}{4\nu_2^2} + \frac{\eta_2^2}{\nu_2}$.
 478 Using the dependence on k , the convergence factor becomes

$$479 \quad \rho(k, \sigma_1, \sigma_2) = \frac{\nu_2 \sqrt{k^2 + \delta^2} + \frac{a_1}{2} - \sigma_1(k)}{\nu_1 \sqrt{\tilde{\eta}_1^2 + k^2} + \sigma_1(k)} \frac{\nu_1 \sqrt{\tilde{\eta}_1^2 + k^2} - \sigma_2(k)}{\nu_2 \sqrt{k^2 + \delta^2} + \frac{a_1}{2} + \sigma_2(k)}.$$

480 We can define the two optimal operators S_j^{opt} associated to the eigenvalues $\sigma_1^{\text{opt}}(k) :=$
 481 $\nu_2 \sqrt{k^2 + \delta^2} + \frac{a_1}{2}$ and $\sigma_2^{\text{opt}}(k) := \nu_1 \sqrt{k^2 + \tilde{\eta}_1^2}$ which lead to convergence in just two
 482 iterations.

483 **3.1. Zeroth order single sided optimized transmission conditions.** Fol-
 484 lowing the strategy of the previous section, we choose $\sigma_1(k), \sigma_2(k)$ so that they coincide
 485 with the optimal choice for the frequency $k = p$, i.e. $\sigma_1(k) = \nu_2 \sqrt{p^2 + \delta^2} + \frac{a_1}{2}$ and
 486 $\sigma_2(k) = \nu_1 \sqrt{p^2 + \tilde{\eta}_1^2}$. Defining $\lambda := \frac{\nu_1}{\nu_2}$, the convergence factor then becomes

$$487 \quad (3.2) \quad \rho(k, p) = \frac{\sqrt{k^2 + \tilde{\eta}_1^2} - \sqrt{p^2 + \tilde{\eta}_1^2}}{\frac{1}{\lambda} \left(\sqrt{k^2 + \delta^2} + \frac{a_1}{2\nu_2} \right) + \sqrt{p^2 + \tilde{\eta}_1^2}} \cdot \frac{\sqrt{k^2 + \delta^2} - \sqrt{p^2 + \delta^2}}{\lambda \sqrt{k^2 + \tilde{\eta}_1^2} + \left(\sqrt{p^2 + \delta^2} + \frac{a_1}{2\nu_2} \right)}.$$

488

489 **THEOREM 3.1.** *The unique optimized Robin parameter p^* solving the min-max*
 490 *problem*

$$491 \quad \min_{p \in \mathbb{R}} \max_{k_{\min} \leq k \leq k_{\max}} |\rho(k, p)|,$$

492 *is given by the unique root of the non linear equation*

$$493 \quad |\rho(p^*, k_{\min})| = |\rho(p^*, k_{\max})|.$$

494 *Proof.* The proof is very similar to the proof of Theorem 2.3, therefore we just
 495 sketch the main steps. We start observing that $\rho(k, p)$ has only one zero located at
 496 $k = p$ and $\rho(k, p) > 0 \quad \forall k, p$. Thus we may neglect the absolute value. Analysing the
 497 derivative with respect to p , we find

$$498 \quad \text{sign} \left(\frac{\partial \rho(k, p)}{\partial p} \right) = -\text{sign}(k - p).$$

499 This implies that $\frac{\partial \rho(k, p)}{\partial p} > 0$ if $k < p$ and $\frac{\partial \rho(k, p)}{\partial p} < 0$ if $k > p$. We conclude that p
 500 must lie in the interval $[k_{\min}, k_{\max}]$. Similarly the derivative with respect to k satisfies

501 $\frac{\partial \rho(k,p)}{\partial k} < 0$ if $k < p$ and $\frac{\partial \rho(k,p)}{\partial k} > 0$ if $k > p$. Hence, the local maxima with respect
 502 to k are located at the boundary points $k = k_{\min}$ and $k = k_{\max}$. Repeating the final
 503 argument of Theorem 2.3 we get the result. \square

504 Since a closed form formula is again not available, we show now asymptotic results
 505 for the optimal parameter p^* and observe the behaviour of the method when taking
 506 finer and finer meshes.

507 **THEOREM 3.2.** *If the physical parameters are fixed, $k_{\max} = \frac{\pi}{h}$ and h is small enough,*
 508 *then the optimized Robin parameter p^* satisfies*

$$509 \quad p^* \sim C_a \cdot h^{-\frac{1}{2}}, \quad C_a = \frac{\sqrt{\nu_2 (\lambda + 1) \pi \left(2 \sqrt{k_{\min}^2 + \tilde{\eta}_1^2 \lambda \nu_2} + 2 \sqrt{k_{\min}^2 + \delta^2 \nu_2} - a_1 \right)}}{\sqrt{2} \nu_2 (\lambda + 1)}.$$

510 *Furthermore the asymptotic convergence factor is*

$$511 \quad \max_{k_{\min} \leq k \leq \pi/h} |\rho(k, p^*)| \sim 1 - h^{\frac{1}{2}} \left(\frac{C_a (\lambda + 1)^2}{\lambda \pi} \right).$$

512 *Proof.* We insert the ansatz $p = C_a \cdot h^{-\alpha}$ into the equation (2.12). Expanding for
 513 small h , we get that

$$514 \quad \rho(p, k_{\min}) \sim 1 - h^\alpha \left(\frac{C_a (\lambda + 1)^2}{\lambda \pi} \right).$$

515 On the other hand,

$$516 \quad \rho(p, k_{\max}) \sim 1 + h^{-\alpha+1} \left(\frac{1}{2} \frac{(\lambda + 1) \left(-2 \sqrt{k_{\min}^2 + \tilde{\eta}_1^2 \lambda \nu_2} - 2 \sqrt{k_{\min}^2 + \delta^2 \nu_2} + a_1 \right)}{C_a \nu_2 \lambda} \right).$$

517 Comparing the first two terms we get the result. \square

518 **3.2. Zeroth order two sided optimized transmission conditions.** In this
 519 paragraph we generalize the previous transmission conditions, introducing another
 520 degree of freedom q . The operators S_j are such that their eigenvalues are

$$521 \quad \sigma_1(k) = \nu_2 \sqrt{q^2 + \delta^2} + \frac{a_1}{2}, \quad \sigma_2(k) = \nu_1 \sqrt{p^2 + \tilde{\eta}_1^2},$$

522 and the convergence factor becomes

$$523 \quad \rho(k, p) = \frac{\sqrt{k^2 + \tilde{\eta}_1^2} - \sqrt{p^2 + \tilde{\eta}_1^2}}{\frac{1}{\lambda} \left(\sqrt{k^2 + \delta^2} + \frac{a_1}{2\nu_2} \right) + \sqrt{p^2 + \tilde{\eta}_1^2}} \cdot \frac{\sqrt{k^2 + \delta^2} - \sqrt{q^2 + \delta^2}}{\lambda \sqrt{k^2 + \tilde{\eta}_1^2} + \left(\sqrt{q^2 + \delta^2} + \frac{a_1}{2\nu_2} \right)}.$$

524 In order to prove a similar result as in Theorem 2.10, we suppose that $\tilde{\eta}_1 = 0$, i.e.
 525 only diffusion is present in Ω_1 , and $a_1 > 0$, i.e. the advection flux is pointing into the
 526 subdomain Ω_2 .

527 **THEOREM 3.3.** *There are two pairs of parameters (p_1^*, q_1^*) and (p_2^*, q_2^*) such that*
 528 *we obtain equioscillation between all the three local maxima located at the boundary*
 529 *extrema k_{\min}, k_{\max} and at the interior point \hat{k} ,*

$$530 \quad |\rho(k_{\min}, p_j^*, q_j^*)| = |\rho(k_{\max}, p_j^*, q_j^*)| = |\rho(\hat{k}, p_j^*, q_j^*)| \quad j = 1, 2.$$

531 *The optimal pair of parameters is the one which realizes the*

$$532 \quad \min_{(p_j^*, q_j^*), j=1,2} |\rho(k_{\min}, p_j^*, q_j^*)|.$$

533 *Proof.* Similarly to the proof of Theorem 2.10, we observe that the function admits
 534 two zeros, one located at $k = p$, the other at $k = q$ due to the choice of the transmission
 535 operators. Computing the derivatives with respect to p and q we get

$$536 \quad \begin{aligned} \text{sign}\left(\frac{\partial|\rho|}{\partial p}\right) &= -\text{sign}(\rho) \cdot \text{sign}(k - q) = -\text{sign}(k - p), \\ \text{sign}\left(\frac{\partial|\rho|}{\partial q}\right) &= -\text{sign}(\rho) \cdot \text{sign}(k - p) = -\text{sign}(k - q). \end{aligned}$$

537 We conclude that, at the optimum, both p and q lie in $[k_{\min}, k_{\max}]$, i.e. the function at
 538 the optimum has two zeros in the interval. Now we study the behaviour with respect
 539 to k . Computing the derivative with respect to k , we find that the potential local
 540 maxima are given by the roots of

$$541 \quad \frac{\sqrt{\delta^2 + k^2} - \sqrt{\delta^2 + q^2}}{k(\lambda k + \sqrt{q^2 + \delta^2} + \frac{a_1}{2\nu_2})} = \frac{p - k}{\sqrt{k^2 + \delta^2} \left(p\lambda + \sqrt{k^2 + \delta^2} + \frac{a_1}{2\nu_2} \right)}.$$

542 With some algebraic manipulations, we find that a sufficient condition such that
 543 $\frac{p-k}{(p\lambda + \sqrt{k^2 + \delta^2} + \frac{a_1}{2\nu_2})}$ has a monotonic behaviour with respect to k is that $a_1 > 0$.
 544 Then under this hypothesis we may repeat the arguments in the proof of Theorem
 545 2.10. Letting p, q in $[k_{\min}, k_{\max}]$, we have that the local maxima of the function are
 546 located at $k_{\min}, k_{\max}, \hat{k}$. Moreover we have

$$547 \quad \begin{aligned} \frac{\partial|\rho|}{\partial p} \Big|_{k=k_{\min}} &> 0, & \frac{\partial|\rho|}{\partial q} \Big|_{k=k_{\min}} &> 0, \\ 548 \quad (3.3) \quad \frac{\partial|\rho|}{\partial p} \Big|_{k=k_{\max}} &< 0, & \frac{\partial|\rho|}{\partial q} \Big|_{k=k_{\max}} &< 0, \\ 549 \quad \frac{\partial|\rho|}{\partial p} \Big|_{k=\hat{k}} &< 0, & \frac{\partial|\rho|}{\partial q} \Big|_{k=\hat{k}} &> 0. \end{aligned}$$

551 We can thus repeat the same arguments as in the proof of Theorem 2.10 since all
 552 steps are now exclusively based on the sign of the partial derivatives with respect to
 553 the parameters, see (3.3), and the result follows. \square

554 **THEOREM 3.4.** *Let $D := \sqrt{k_{\min}^2 + \delta^2}$. If the physical parameters $\tilde{\eta}_2^2, \nu_1, \nu_2, a_1$ are*
 555 *fixed, $k_{\max} = \frac{\pi}{h}$ and h goes to zero, the optimized two-sided Robin parameters are for*
 556 *$\lambda \geq 1$,*

$$557 \quad p_1^* \sim P_1 h^{-1} + E_1 h^{-\frac{1}{2}}, \quad q_1^* \sim Q_1 - F_1 h^{\frac{1}{2}}, \quad \max_{k_{\min} \leq k \leq \frac{\pi}{h}} |\rho(k, p_1^*, q_1^*)| \sim \lambda - \frac{E_1 \pi (\lambda + 1)}{(P_1 \lambda + \pi)^2} h^{\frac{1}{2}},$$

558 with

$$559 \quad P_1 := \frac{\pi(\lambda-1)}{2\lambda}, \quad Q_1 := \sqrt{\frac{D + k_{\min} + \frac{a_1}{2\nu_2\lambda}}{1 - \frac{1}{\lambda}}} - \delta^2,$$

$$560 \quad E_1 := \frac{(2(P_1\sqrt{\delta^2 + Q_1^2} + C_h^2)(\lambda+1)\nu_2 + P_1 a_1)(\lambda P_1 + \pi)^2}{2\lambda^2 P_1 \nu_2 C_h \pi (\lambda+1)},$$

$$561 \quad F_1 := \frac{(2(P_1\sqrt{\delta^2 + Q_1^2} + C_h^2)(\lambda+1)\nu_2 + P_1 a_1)(2\nu_2(\lambda k_{\min} + \sqrt{\delta^2 + Q_1^2}) + a_1)^2 \sqrt{\delta^2 + Q_1^2}}{4\lambda^2 P_1 \nu_2^2 C_h Q_1 (2\nu_2(\lambda k_{\min} + D) + a_1)},$$

$$562 \quad C_h := \frac{\sqrt{P_1(2\sqrt{\delta^2 + Q_1^2}\nu_2(\lambda+1) + a_1)}}{\sqrt{2\nu_2(\lambda+1)}}.$$

563 and for $\lambda < 1$,

$$565 \quad p_2^* \sim P_2 - E_2 h^{\frac{1}{2}}, \quad q_2^* \sim Q_2 h^{-1} + F_2 h^{-\frac{1}{2}}, \quad \max_{k_{\min} \leq k \leq \frac{\pi}{h}} |\rho(k, p_2^*, q_2^*)| \sim \lambda - \frac{F_2 \lambda \pi (1+\lambda)}{(\lambda \pi + Q_2)^2} h^{\frac{1}{2}}.$$

566 with

$$567 \quad P_2 := \frac{D + k_{\min} + \frac{a_1}{2\nu_2}}{1 - \lambda}, \quad Q_2 := \frac{\pi(\lambda-1)}{2},$$

$$568 \quad E_2 := \frac{((\lambda+1)(D_h^2 + P_2 Q_2)\nu_2 + \frac{a_1 Q_2}{2})(2\nu_2(\lambda P_2 + D) + a_1)^2}{2\nu_2^2 D_h Q_2 (2k_{\min} \lambda \nu_2 + 2\nu_2 D + a_1)},$$

$$569 \quad F_2 := \frac{\sqrt{\lambda+1} \sqrt{(D + k_{\min})(\lambda+1) + \frac{a_1}{2\nu_2}} \sqrt{\pi(3\lambda-1)^2}}{\sqrt{2}(1-\lambda^2)},$$

$$570 \quad D_h := \frac{\sqrt{Q_2(2P_2\nu_2(\lambda+1) + a_1)}}{\sqrt{2\nu_2(\lambda+1)}}.$$

571 *Proof.* The proof follows the same steps as in the proof of Theorem 2.11. \square

573 **3.3. Advection tangential to the interface.** In the previous subsection we
 574 restricted our study to the case of advection normal to the interface. Here we consider
 575 the other relevant physical case, namely advection tangential to the interface, so that
 576 $a_1 = 0$ and $a_2 \neq 0$ in (3.1). For homogeneous problems, this case has been studied
 577 through Fourier transform in unbounded domains, see for instance [7]. However, it
 578 has recently been observed in [18], that for homogeneous problems with tangential
 579 advection this procedure does not yield efficient optimized parameters. The reason
 580 behind this failure lies in the separation of variables technique which applied to the
 581 error equation,

$$582 \quad (3.4) \quad \begin{aligned} (\eta_1^2 - \nu_1 \Delta) e_1^n &= 0, \quad \text{in } \Omega_1, \\ (\nu_1 \partial_x + S_1)(e_1^n)(0, \cdot) &= (\nu_2 \partial_x + S_1)(e_2^{n-1})(0, \cdot), \\ (\eta_2^2 + a_2 \partial_y - \nu_2 \Delta) e_2^n &= 0, \quad \text{in } \Omega_2, \\ (\nu_2 \partial_x - S_2)(e_2^n)(0, \cdot) &= (\nu_1 \partial_x - S_2)(e_1^{n-1})(0, \cdot), \end{aligned}$$

583 leads to

$$584 \quad (3.5) \quad e_1^n = \sum_{k \in \mathcal{V}} \hat{e}_1^n(0, k) e^{\lambda_1(k)x} \sin(ky) \quad \text{and} \quad e_2^n = \sum_{k \in \mathcal{V}} \hat{e}_2^n(0, k) e^{-\lambda_2(k)x} e^{\frac{a_2 y}{2\nu_2}} \sin(ky),$$

585 where $\lambda_1(k) = \sqrt{k^2 + \tilde{\eta}_1}$, $\lambda_2(k) = \frac{\sqrt{4\nu_2^2 k^2 + 4\nu_2^2 \tilde{\eta}_2^2 + a_2^2}}{2\nu_2}$ with $\tilde{\eta}_j^2 := \frac{\eta_j^2}{\nu_j}$. Since the func-
 586 tions $\psi_k(y) := \sin(ky)$ and $\phi_k(y) := e^{\frac{a_2 y}{2\nu_2}} \sin(ky)$ are not orthogonal, it is not possible

587 to obtain a recurrence relation which expresses $\hat{e}_j^n(0, k)$ only as a function of $\hat{e}_j^{n-2}(0, k)$
 588 for each k and $j = 1, 2$. Nevertheless we here propose a more general approach. First
 589 let us define two scalar products, the classical L^2 scalar product $\langle f, g \rangle = \frac{2}{L} \int_{\Gamma} f g dy$ and
 590 the weighted scalar product $\langle f, g \rangle_w = \frac{2}{L} \int_{\Gamma} f g e^{-\frac{\alpha_2 y}{\nu_2}} dy$. It follows that $\langle \psi_k, \psi_j \rangle = \delta_{k,j}$
 591 and $\langle \phi_k, \phi_j \rangle_w = \delta_{k,j}$. Setting $S_1 := \nu_2 \lambda_2(p)$ and $S_2 := \nu_1 \lambda_1(q)$ for $p, q \in \mathbb{R}$ and
 592 inserting the expansions (3.5) into the boundary conditions of (3.4) we obtain
 (3.6)

$$\begin{aligned}
 \sum_{i=1}^{+\infty} \hat{e}_1^n(0, i) (\nu_1 \lambda_1(i) + \nu_2 \lambda_2(p)) \psi_i(y) &= \sum_{l=1}^{+\infty} \hat{e}_2^{n-1}(0, l) (-\nu_2 \lambda_2(l) + \nu_2 \lambda_2(p)) \phi_l(y), \\
 \sum_{l=1}^{+\infty} \hat{e}_2^n(0, l) (-\nu_2 \lambda_2(l) - \nu_1 \lambda_1(q)) \phi_l(y) &= \sum_{i=1}^{+\infty} \hat{e}_1^{n-1}(0, i) (\nu_1 \lambda_1(i) - \nu_1 \lambda_1(q)) \psi_i(y).
 \end{aligned}$$

594 We truncate the expansions for $i, l > N$, since higher frequencies are not represented
 595 by the numerical grid, and we project the first equation onto ψ_k with respect the
 596 scalar product $\langle \cdot, \cdot \rangle$ and the second one onto ϕ_j with respect to the weighted scalar
 597 product $\langle \cdot, \cdot \rangle_w$,
 (3.7)

$$\begin{aligned}
 \hat{e}_1^n(0, k) (\nu_1 \lambda_1(k) + \nu_2 \lambda_2(p)) &= \sum_{l=1}^N \hat{e}_2^{n-1}(0, l) (-\nu_2 \lambda_2(l) + \nu_2 \lambda_2(p)) \langle \psi_k, \phi_l \rangle, \\
 \hat{e}_2^n(0, j) (-\nu_2 \lambda_2(j) - \nu_1 \lambda_1(q)) &= \sum_{i=1}^N \hat{e}_1^{n-1}(0, i) (\nu_1 \lambda_1(i) - \nu_1 \lambda_1(q)) \langle \phi_j, \psi_i \rangle_w.
 \end{aligned}$$

599 Defining now the vectors $\mathbf{e}_j^n \in \mathbb{R}^N$ such that $(\mathbf{e}_j^n)_i := \hat{e}_j^n(0, i)$ for $j = 1, 2$, the matrices
 600 $V_{k,l} := \langle \psi_k, \phi_l \rangle$, $W_{j,i} := \langle \phi_j, \psi_i \rangle_w$ and the diagonal matrices $(D_1)_{l,l} := (-\nu_2 \lambda_2(l) +$
 601 $\nu_2 \lambda_2(p))$, $(\tilde{D}_1)_{k,k} := (\nu_1 \lambda_1(k) + \nu_2 \lambda_2(p))$, $(D_2)_{i,i} := (\nu_1 \lambda_1(i) - \nu_1 \lambda_1(q))$, $(\tilde{D}_2)_{j,j} :=$
 602 $(-\nu_2 \lambda_2(j) - \nu_1 \lambda_1(q))$, we obtain,

$$\begin{aligned}
 \mathbf{e}_1^n &= \tilde{D}_1^{-1} V D_1 \mathbf{e}_2^{n-1}, \\
 \mathbf{e}_2^n &= \tilde{D}_2^{-1} W D_2 \mathbf{e}_1^{n-1},
 \end{aligned}$$

604 which implies

$$(3.9) \quad \mathbf{e}_1^n = \tilde{D}_1^{-1} V D_1 \tilde{D}_2^{-1} W D_2 \mathbf{e}_1^{n-2} \text{ and } \mathbf{e}_2^n = \tilde{D}_2^{-1} W D_2 \tilde{D}_1^{-1} V D_1 \mathbf{e}_2^{n-2}.$$

606 Since for two given matrices A, B the spectral radius satisfies $\rho(AB) = \rho(BA)$, we
 607 conclude that $\rho(\tilde{D}_1^{-1} V D_1 \tilde{D}_2^{-1} W D_2) = \rho(\tilde{D}_2^{-1} W D_2 \tilde{D}_1^{-1} V D_1)$ and therefore, in order
 608 to accelerate the method, we are interested in the minimization problem

$$(3.10) \quad \min_{p, q \in \mathbb{R}} \rho((\tilde{D}_1^{-1} V D_1 \tilde{D}_2^{-1} W D_2)(p, q)).$$

610 Problem (3.10) does not have yet a closed formula solution. However in the next
 611 section we show its efficiency by solving numerically the minimization problem.

612 *Remark 3.5.* Equation (3.10) is a straight generalization of the min-max prob-
 613 lem (2.8). Indeed, assuming that the functions ψ_k and ϕ_j are orthogonal, the ma-
 614 trices V and W are the identity matrix. Therefore equation (3.9) simplifies to
 615 $\mathbf{e}_1^n = \tilde{D}_1 \mathbf{e}_1^{n-2}$ and $\mathbf{e}_2^n = \tilde{D}_2 \mathbf{e}_2^{n-2}$, where the diagonal matrix \tilde{D} satisfies $(\tilde{D})_{k,k} =$
 616 $\frac{\nu_2 \lambda_2(k) - \nu_2 \lambda_2(p)}{\nu_1 \lambda_1(k) + \nu_2 \lambda_2(p)} \frac{\nu_1 \lambda_1(k) - \nu_1 \lambda_1(q)}{\nu_2 \lambda_2(k) + \nu_1 \lambda_1(q)}$. Since the eigenvalues of a diagonal matrix are its diag-
 617 onal entries we get that if $W = V = I$,

$$618 \min_{p, q \in \mathbb{R}} \rho((\tilde{D}_1^{-1} V D_1 \tilde{D}_2^{-1} W D_2)(p, q)) = \min_{p, q} \max_k \left| \frac{\nu_2 \lambda_2(k) - \nu_2 \lambda_2(p)}{\nu_1 \lambda_1(k) + \nu_2 \lambda_2(p)} \frac{\nu_1 \lambda_1(k) - \nu_1 \lambda_1(q)}{\nu_2 \lambda_2(k) + \nu_1 \lambda_1(q)} \right|.$$

h	ρ single sided	ρ double sided	h	ρ single sided	ρ double sided
1/50	0.7035	0.4052	1/50	0.1721	0.0337
1/100	0.7801	0.4748	1/100	0.2625	0.0456
1/500	0.8950	0.6160	1/500	0.4868	0.0685
1/1000	0.9245	0.6672	1/1000	0.5823	0.0760
1/5000	0.9655	0.7650	1/5000	0.7662	0.0872

Table 2: Asymptotic behaviour as $h \rightarrow 0$ for the reaction diffusion-diffusion coupling. Physical parameters: left table $\tilde{\eta}^2 = \lambda = 1$, right table $\tilde{\eta}^2 = \lambda = 10$.

619 *Remark 3.6.* The case of an arbitrary advection, i.e. $a_1 \neq 0$ and $a_2 \neq 0$ has
620 been recently treated in [18] for homogeneous problems. Considering a heterogeneous
621 problem with advection fields $\mathbf{a}_j = (a_{1j}, a_{2j})^\top$ in domain Ω_j , $j = 1, 2$, a separation
622 of variables approach would lead to non orthogonal functions $\psi_k(y) = e^{\frac{a_{21}y}{2\nu_1}} \sin(ky)$
623 and $\phi_k(y) = e^{\frac{a_{22}y}{2\nu_2}} \sin(ky)$ unless $\frac{a_{21}}{2\nu_1} = \frac{a_{22}}{2\nu_2}$, and thus it is not possible to obtain a
624 recurrence relation as shown in (3.5). However the approach developed in this section
625 can be readily applied. The subdomain solutions are

$$626 \quad e_1^n(x, y) = \sum_{k \in \mathcal{V}} \hat{e}_{1,k}^n e^{\frac{a_{21}y}{2\nu_1}} \sin(ky) e^{\lambda_1(k)x}, \quad e_2^n(x, y) = \sum_{k \in \mathcal{V}} \hat{e}_{2,k}^n e^{\frac{a_{22}y}{2\nu_2}} \sin(ky) e^{-\lambda_2(k)x},$$

627 with $\lambda_1(k) = \frac{a_{11} + \sqrt{4\nu_1^2 k^2 + 4\nu_1^2 \tilde{\eta}_1^2 + a_{11}^2 + a_{21}^2}}{2\nu_1}$ and $\lambda_2(k) = \frac{-a_{12} + \sqrt{4\nu_2^2 k^2 + 4\nu_2^2 \tilde{\eta}_2^2 + a_{12}^2 + a_{22}^2}}{2\nu_2}$.
628 Defining $S_1 = \nu_2 \lambda_2(p) + a_{12}$, $S_2 = \nu_1 \lambda_1(p) - a_{11}$, the two scalar products $\langle f, g \rangle_{w_1} =$
629 $\frac{2}{L} \int_{\Gamma} f g e^{-\frac{a_{21}y}{\nu_1}} dy$ and $\langle f, g \rangle_{w_2} = \frac{2}{L} \int_{\Gamma} f g e^{-\frac{a_{22}y}{\nu_2}} dy$ and repeating the calculations (3.6)-
630 (3.8), one finds the recurrence relation (3.9), with $V_{k,l} := \langle \psi_k, \phi_l \rangle_{w_1}$, $W_{j,i} := \langle \phi_j, \psi_i \rangle_{w_2}$
631 and the diagonal matrices $(D_1)_{l,l} := (-\nu_2 \lambda_2(l) + \nu_2 \lambda_2(p))$, $(\tilde{D}_1)_{k,k} := (\nu_1 \lambda_1(k) +$
632 $\nu_2 \lambda_2(p) - a_{11} + a_{12})$, $(D_2)_{i,i} := (\nu_1 \lambda_1(i) - \nu_1 \lambda_1(q))$, $(\tilde{D}_2)_{j,j} := (-\nu_2 \lambda_2(j) - \nu_1 \lambda_1(q) -$
633 $a_{12} + a_{11})$.

634 **4. Numerical results.** Our numerical experiments to test the different coupling
635 strategies separately are performed using the subdomains $\Omega_1 = (-1, 0) \times (0, 1)$, $\Omega_2 =$
636 $(0, 1) \times (0, 1)$. We use a classical five point finite difference scheme for the interior
637 points and treat the normal derivatives with second order discretization using a ghost
638 point formulation.

639 **4.1. Reaction Diffusion-Diffusion coupling.** We first consider the reaction
640 diffusion-diffusion coupling analyzed in Section 2. Tables 2 and 3 show the values
641 of the convergence factor in two different asymptotic regimes, when $h \rightarrow 0$, and
642 for strong heterogeneity. As the asymptotic Theorem 2.11 and Remark 2.5 state, a
643 strong heterogeneity improves the performance of the algorithm. In the single sided
644 optimized case, the value of the convergence factor $|\rho(k)|$ tends to 1, while in the
645 double sided case, $|\rho(k)|$ is bounded either by λ or by $1/\lambda$. Fig. 4 shows the number
646 of iterations required to reach convergence with a tolerance of 10^{-6} as function of
647 the optimized parameters in both the single and double sided cases. We see that the
648 analysis predicts the optimized parameter very well.

649 **4.2. Advection Reaction Diffusion-Diffusion coupling.** Next we consider
650 the advection reaction diffusion-diffusion coupling with advection normal to the inter-
651 face. Table 4 summarizes the behaviour of $\rho(k)$ as $h \rightarrow 0$ and for strong heterogeneity.

λ	ρ single sided	ρ double sided
0.001	0.0125	$7.8 \cdot 10^{-4}$
0.01	0.1075	0.0078
0.1	0.4453	0.0757
1	0.5851	0.4748
10	0.2625	0.076
100	0.0389	0.0078
1000	0.0040	$7.8 \cdot 10^{-4}$

Table 3: Asymptotic behaviour as $\lambda \rightarrow 0$ and $\lambda \rightarrow \infty$, with $h = 0.05$ for the reaction diffusion-diffusion coupling. Physical parameter: $\tilde{\eta}^2 = 1$.

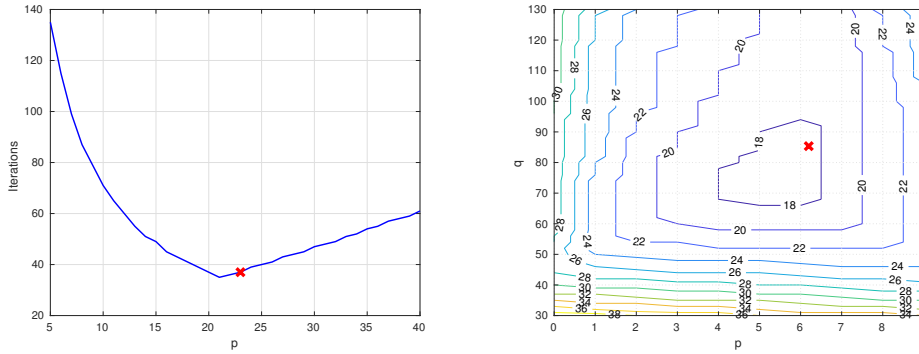


Fig. 4: Number of iterations required to reach convergence with a tolerance of 10^{-6} as function of the optimized parameters for the reaction diffusion-diffusion coupling. The left panel shows the single sided case while the right panel shows the double sided case. Physical parameters : $\nu_1 = 2$, $\nu_2 = 1$, $\eta^2 = 10$, mesh size $h = 0.02$.

652 Similarly Fig 5 shows the number of iterations required to reach convergence with the
 653 tolerance of 10^{-6} . Figure 6 shows the number of iterations to reach convergence for the
 654 tangential advection case. The minimization problem (3.10) is solved numerically to
 655 find the optimal parameters p and q using the Nelder-Mead algorithm. We have solved
 656 the minimization problem with different initial couples (p, q) and we have noticed that
 657 the optimal solution satisfies an ordering relation between p and q depending on λ as
 658 in Theorem 2.11 and 3.4.

659 **4.3. Application to the contaminant transport problem.** The compu-
 660 tational domain Ω described in Fig 1 is set equal to $\Omega = (0, 8) \times (-4, 0)$, with
 661 $\Omega_j = (0, 8) \times (1 - j, -j)$, $j = 1 \dots 4$. On the top boundary Γ_1 , we impose a condi-
 662 tion on the incoming contaminant flow, i.e. $\frac{\partial u}{\partial y} - a_2 u = 1$ while on the bottom edge
 663 Γ_3 we impose a zero Neumann boundary condition $\frac{\partial u}{\partial y} = 0$. On the vertical edges Γ_2
 664 and Γ_4 we set absorbing boundary conditions so that

$$665 \quad \begin{aligned} \frac{\partial u}{\partial \mathbf{n}} + pu &= 0 & \text{on } \{0\} \times [-3; 0] \text{ and } \{8\} \times [-3; 0], \\ \frac{\partial u}{\partial \mathbf{n}} - a_1 u + pu &= 0 & \text{on } \{0\} \times [-4; -3] \text{ and } \{8\} \times [-4; -3], \end{aligned}$$

h	ρ single sided	ρ double sided	λ	ρ single sided	ρ double sided
1/50	0.4766	0.1835	0.001	0.0031	$4.89 \cdot 10^{-4}$
1/100	0.5910	0.2306	0.01	0.0297	0.0049
1/500	0.7889	0.3274	0.1	0.2101	0.0458
1/1000	0.8452	0.3618	1	0.4865	0.2552
1/5000	0.9273	0.4228	10	0.2786	0.0517
			100	0.0459	0.0056
			1000	0.0049	$5.6 \cdot 10^{-4}$

Table 4: For the advection reaction diffusion-diffusion coupling, the left table shows the asymptotic behaviour when $h \rightarrow 0$ while the right table shows the values of the convergence factor for strong heterogeneity when $h = 1/50$. Physical parameters: $\eta_1^2 = 1, \eta_2^2 = 2, \nu_1 = 2, \nu_2 = 1, a_2 = 0, a_1 = 5$, mesh size $h = 0.02$.

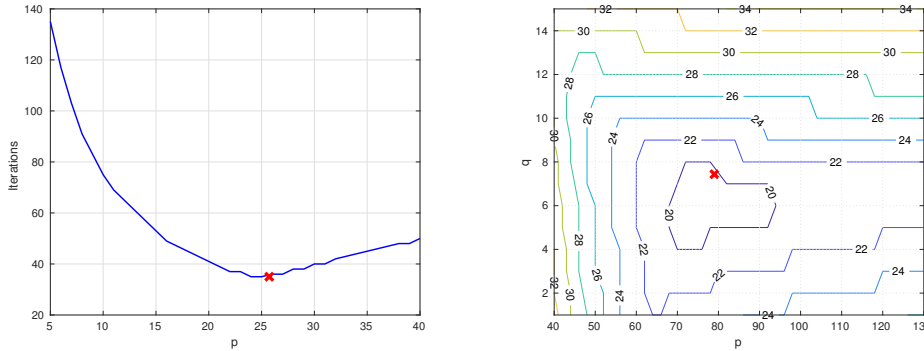


Fig. 5: Number of iterations required to reach convergence with a tolerance of 10^{-6} as function of the optimized parameters for the advection reaction diffusion-diffusion coupling with normal advection. Physical parameters: $\nu_1 = 2, \nu_2 = 1, \eta_1^2 = 1, \eta_2^2 = 2, a_1 = 5$, mesh size $h = 0.02$.

666 where \mathbf{n} is the outgoing normal vector. The parameter p is chosen equal to $p = \sqrt{\pi \frac{\pi}{h}}$,
667 being $k_{\min} = \pi$ and $k_{\max} = \frac{\pi}{h}$. This choice derives from the observation that imposing
668 $\frac{\partial u}{\partial n} + DtNu = 0$, where DtN is the Dirichlet to Neumann operator, is an exact
669 transparent boundary condition, see [29, 28]. Thus we replace the expensive exact
670 transparent boundary condition with an approximation of the DtN operator. We
671 know from [9] that $p = \sqrt{\pi \frac{\pi}{h}}$ is indeed a zero order approximation of the DtN

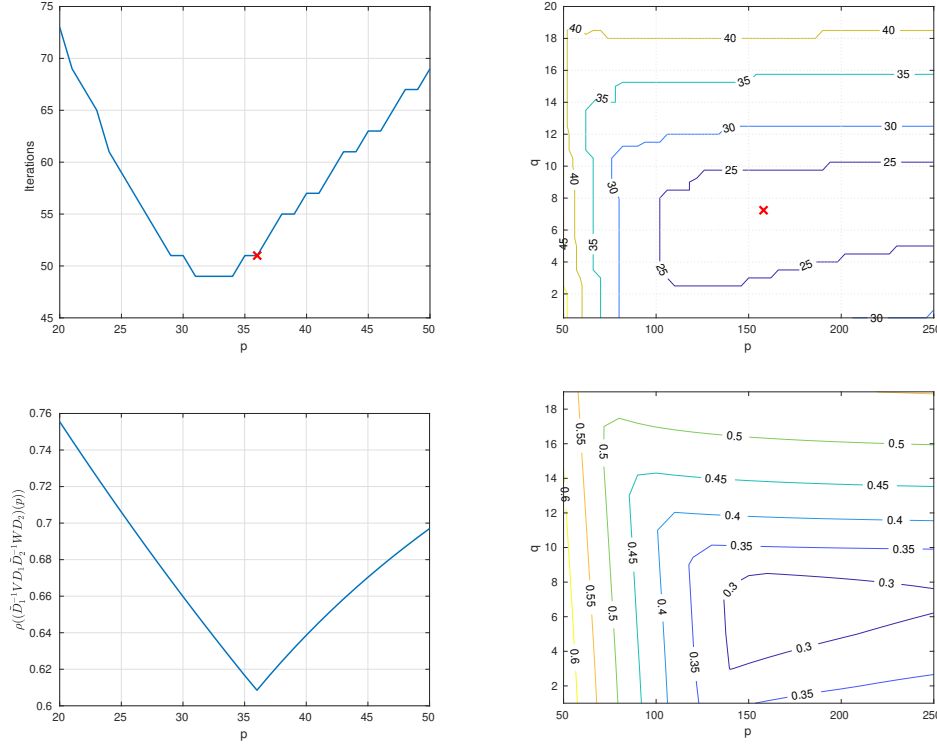


Fig. 6: In the top row, we show the number of iterations required to reach convergence with a tolerance of 10^{-6} as function of the optimized parameters for the advection reaction diffusion-diffusion coupling with tangential advection. In the bottom row, we show the dependence on p and the level curves of the objective function in the min-max problem (3.10). Physical parameters: $\nu_1 = 1$, $\nu_2 = 2$, $\eta_1^2 = 1$, $\eta_2^2 = 2$, $a_2 = 15$, mesh size $h = 0.01$.

672 operator. To solve the system of PDEs, we consider the optimized Schwarz method:
 (4.1)

$$\begin{aligned}
 -\nu_1 \Delta u_1^n - a_2 \partial_y u_1^n &= 0 & \text{in } \Omega_1, & \mathcal{B}_1(u_1^n) = 0 \text{ on } \partial\Omega_1 \setminus \Sigma_1, \\
 \partial_{n_{1,2}} u_1^n + p_{12} u_1^n &= \partial_{n_{1,2}} u_2^{n-1} + p_{12} u_2^{n-1} & \text{on } \Sigma_1, & \\
 \eta_2^2 u_2^n - \nu_2 \Delta u_2^n &= 0 & \text{in } \Omega_2, & \mathcal{B}_2(u_2^n) = 0 \text{ on } \partial\Omega_2 \setminus \{\Sigma_1, \Sigma_2\}, \\
 \partial_{n_{1,1}} u_2^n + p_{21} u_2^n &= \partial_{n_{1,1}} u_1^{n-1} + p_{21} u_1^{n-1} & \text{on } \Sigma_1, & \\
 \partial_{n_{2,3}} u_2^n + p_{23} u_2^n &= \partial_{n_{2,3}} u_3^{n-1} + p_{23} u_3^{n-1} & \text{on } \Sigma_2, & \\
 -\nu_3 \Delta u_3^n &= 0 & \text{in } \Omega_3, & \mathcal{B}_3(u_3^n) = 0 \text{ on } \partial\Omega_3 \setminus \{\Sigma_2, \Sigma_3\}, \\
 \partial_{n_{2,2}} u_3^n + p_{32} u_3^n &= \partial_{n_{2,2}} u_2^{n-1} + p_{32} u_2^{n-1} & \text{on } \Sigma_2, & \\
 \partial_{n_{3,4}} u_3^n + p_{34} u_3^n &= \partial_{n_{3,4}} u_4^{n-1} + p_{34} u_4^{n-1} & \text{on } \Sigma_3, & \\
 -\nu_4 \Delta u_4^n + a_1 \partial_x u_4^n &= 0 & \text{in } \Omega_4, & \mathcal{B}_4(u_4^n) = 0 \text{ on } \partial\Omega_4 \setminus \Sigma_3, \\
 \partial_{n_{3,3}} u_4^n + p_{43} u_4^n &= \partial_{n_{3,3}} u_3^{n-1} + p_{43} u_3^{n-1} & \text{on } \Sigma_3, &
 \end{aligned}$$

674 where Σ_i are the shared interfaces $\Sigma_i = \partial\Omega_i \cap \partial\Omega_{i+1}$, $i = 1, 2, 3$, the vectors $\mathbf{n}_{i,j}$ are
 675 the normal vectors on the interface Σ_i pointing towards the interior of the domain Ω_j
 676 and the operators $\mathcal{B}_i(u_i)$ represent the boundary conditions to impose on the bound-
 677 ary excluding the shared interfaces. Regarding the Robin parameters $p_{i,j}$, we choose

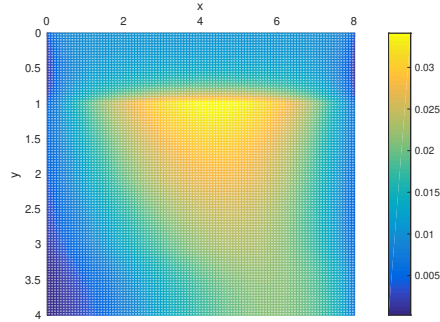


Fig. 7

Stationary distribution of the contaminant. Physical parameters:

$$\nu_1 = 0.5, \nu_2 = 3, \nu_3 = 3, \nu_4 = 1, \eta_2^2 = 0.01, a_2 = 2, a_1 = 2.$$

678 them according to the two subdomain analysis carried out in this manuscript. Due
 679 to the exponential decay of the error away from the interface, see eq. (2.3), if the
 680 subdomains are not too narrow in the y direction, the information transmitted from
 681 each subdomain to the neighbouring one does not change significantly and therefore
 682 the $p_{i,j}$ from a two subdomain analysis are still a good choice. We remark that this ar-
 683 gument does not hold for the Helmholtz equation, for which there are resonant modes
 684 for frequencies $k \leq \omega$, where ω is the wave number, which travel along the domains
 685 and they do not decay away from the interface. Figure 7 shows the stationary distri-
 686 bution of the contaminant. We observe that due to the advection in the y direction
 687 in Ω_1 , the contaminant accumulates on the interface with Ω_2 , representing the porous
 688 medium, and here we have the highest concentration. Then the contaminant diffuses
 689 into the layers below and already in the porous media region it feels the presence of
 690 the tangential advection in Ω_4 . Next we also consider the transient version of equa-
 691 tions (4.1). We discretize the time derivative with an implicit Euler scheme, so that
 692 each equation has a further reaction term equal to $\eta_{j,tran}^2 = \eta_{j,stat}^2 + \frac{1}{\Delta t}$. Figure 8
 693 shows the time dependent evolution of the concentration u over 400 integration steps.
 694 The initial condition is set equal to zero on the whole domain Ω .

695 Table 5 shows the number of iterations to reach a tolerance of 10^{-6} for the al-
 696 gorithm (4.1) both used as iterative method and as a preconditioner for GMRES for
 697 the substructured system, see [13] for an introduction to the substructured version of
 698 (4.1). We consider both single and double sided optimizations for the parameters $p_{i,j}$
 699 at each interface. For the time evolution problem, the stopping criterion is

$$700 \quad (4.2) \quad \max \left\{ \frac{\|u_{1,\Sigma_1}^{n,k} - u_{2,\Sigma_1}^{n,k}\|}{\|u_{1,\Sigma_1}^{n,k}\|}, \frac{\|u_{2,\Sigma_2}^{n,k} - u_{3,\Sigma_2}^{n,k}\|}{\|u_{2,\Sigma_2}^{n,k}\|}, \frac{\|u_{3,\Sigma_3}^{n,k} - u_{4,\Sigma_3}^{n,k}\|}{\|u_{3,\Sigma_3}^{n,k}\|} \right\} \leq 10^{-6}.$$

701 From Figures 7 and 8, we note that this physical configuration would represent a safe
 702 situation since a very small concentration of contaminant manages to get through the
 703 vertical diffusive layers and to reach the right-bottom of the domain, where it could
 704 pollute the water well.

705 **5. Conclusions.** In this manuscript we considered the heterogeneous couplings
 706 arising from second order elliptic PDEs and solved analytically the corresponding

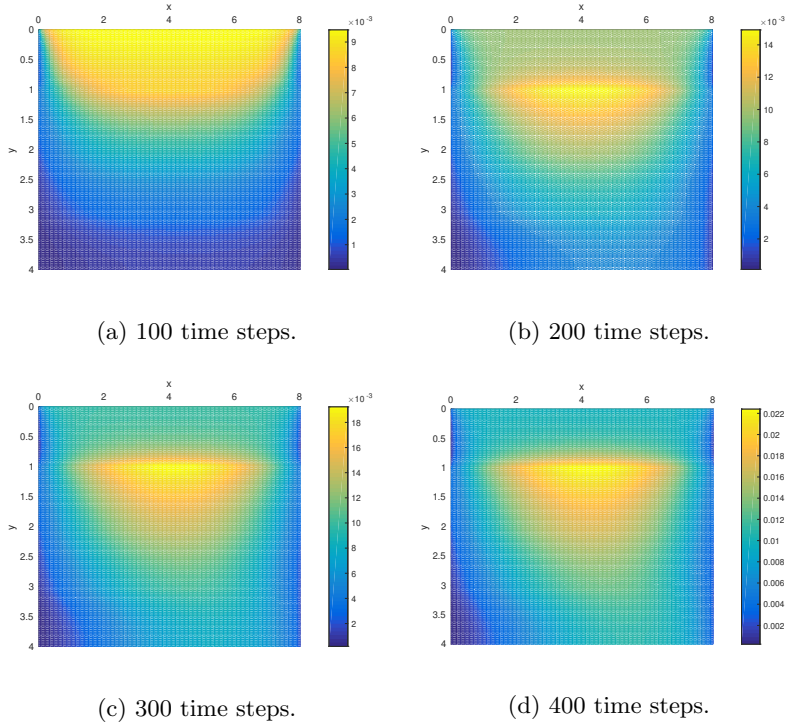


Fig. 8: Evolution of the contaminant concentration u .

	Iterative	GMRES		Iterative	GMRES
Single sided	270	33	Single sided	11.5	5.7
Double sided	55	25	Double sided	9.6	4.3

Table 5

Number of iterations to reach a tolerance of 10^{-6} for the optimized Schwarz method (4.1) used as an iterative method and as a preconditioner. The left side refers to the stationary case while the right side to the transient one where we consider the number of iterations needed to satisfy the stopping criterion (4.2) averaged over 400 time steps.

707 min-max problems, except in the case of tangential advection to the interface where
 708 we provided a numerical optimization procedure. Our results show that optimized
 709 Schwarz methods are not only natural for heterogeneous problems, they are also ex-
 710 tremely efficient. Indeed, the asymptotic analysis shows that the stronger the hetero-
 711 geneity is, the fastest becomes the convergence. In particular, a double sided method
 712 should be preferred since not only is it clearly faster than a single sided one, but it
 713 also leads to an h independent convergence as long as there is a jump in the diffusion
 714 coefficients. Our analysis is based on a two dimensional setting but the results can be
 715 extended to three dimensional problems. Considering $\Omega_1 = (-\infty, 0) \times (0, L) \times (0, \hat{L})$
 716 and $\Omega_2 = (0, +\infty) \times (0, L) \times (0, \hat{L})$, we can obtain analogous sine expansions for the

717 errors e_j^n , $j = 1, 2$ as in Section 2. Then, for symmetric problems and in the case of
 718 normal advection to the plane $\Gamma := \{0\} \times (0, L) \times (0, \hat{L})$, we can reuse the same theo-
 719 retical results by changing the range of frequencies in the min-max problems, setting
 720 $k_{\min} = \frac{\pi}{L} + \frac{\pi}{\hat{L}}$ and $k_{\max} = \frac{2\pi}{h}$. Considering tangential advection, all the possible tan-
 721 gential directions now lie on the plane Γ , which in our example is the y-z plane. Then
 722 one could use the numerical procedure developed in Section 3.3 introducing the matri-
 723 ces V and W and proper scalar products defined as integrals on the 2 dimensional
 724 interface.

725

REFERENCES

- 726 [1] J. BEAR AND A. CHENG, *Modeling Groundwater Flow and Contaminant Transport*, Theory
 727 and Applications of Transport in Porous Media, Springer Netherlands, 2010.
- 728 [2] N. BIRGLE, R. MASSON, AND L. TRENTY, *A domain decomposition method to couple non-*
 729 *isothermal compositional gas liquid Darcy and free gas flows*, accepted in Journal of Com-
 730 putational Physics, (2018).
- 731 [3] E. BLAYO, D. CHEREL, AND A. ROUSSEAU, *Towards optimized Schwarz methods for the Navier-*
 732 *Stokes equations*, Journal of Scientific Computing, 66 (2016), pp. 275–295.
- 733 [4] V. DOLEAN, M. J. GANDER, AND L. GERARDO-GIORDA, *Optimized Schwarz methods for*
 734 *Maxwell’s equations*, SIAM Journal on Scientific Computing, 31 (2009), pp. 2193–2213.
- 735 [5] V. DOLEAN, M. J. GANDER, AND E. VENEROS, *Optimized Schwarz methods for Maxwell equa-*
 736 *tions with discontinuous coefficients*, in Domain Decomposition Methods in Science and
 737 Engineering XXI, Springer, Cham, 2014, pp. 517–525.
- 738 [6] V. DOLEAN AND F. NATAF, *A new domain decomposition method for the compressible Euler*
 739 *equations*, ESAIM: Mathematical Modelling and Numerical Analysis, 40 (2006), p. 689703.
- 740 [7] O. DUBOIS, *Optimized Schwarz methods for the advection-diffusion equation*, PhD thesis, McGill
 741 University, 2007.
- 742 [8] O. DUBOIS, *Optimized Schwarz methods with Robin conditions for the advection-diffusion equa-*
 743 *tion*, Lecture Notes in Computational Science and Engineering, 55 (2007), p. 181.
- 744 [9] M. J. GANDER, *Optimized Schwarz methods*, SIAM Journal on Numerical Analysis, 44 (2006),
 745 pp. 699–731.
- 746 [10] M. J. GANDER, *Schwarz methods over the course of time*, Electron. Trans. Numer. Anal, 31
 747 (2008), pp. 228–255.
- 748 [11] M. J. GANDER, *On the influence of geometry on optimized Schwarz methods*, SeMA Journal,
 749 53 (2011), pp. 71–78.
- 750 [12] M. J. GANDER AND O. DUBOIS, *Optimized Schwarz methods for a diffusion problem with dis-*
 751 *continuous coefficient*, Numerical Algorithms, 69 (2015), pp. 109–144.
- 752 [13] M. J. GANDER AND L. HALPERN, *Méthodes de décomposition de domaine*, Encyclopédie
 753 électronique pour les ingénieurs, (2012).
- 754 [14] M. J. GANDER, L. HALPERN, AND F. MAGOULES, *An optimized Schwarz method with two-*
 755 *sided Robin transmission conditions for the Helmholtz equation*, International journal for
 756 numerical methods in fluids, 55 (2007), pp. 163–175.
- 757 [15] M. J. GANDER, L. HALPERN, AND V. MARTIN, *A new algorithm based on factorization for*
 758 *heterogeneous domain decomposition*, Numerical Algorithms, 73 (2016), pp. 167–195.
- 759 [16] M. J. GANDER, F. MAGOULES, AND F. NATAF, *Optimized Schwarz methods without overlap for*
 760 *the Helmholtz equation*, SIAM Journal on Scientific Computing, 24 (2002), pp. 38–60.
- 761 [17] M. J. GANDER AND T. VANZAN, *Heterogeneous optimized Schwarz methods for coupling*
 762 *Helmholtz and Laplace equations*, in Domain Decomposition Methods in Science and En-
 763 gineering XXIV, Cham, 2018, Springer International Publishing, pp. 311–320.
- 764 [18] M. J. GANDER AND T. VANZAN, *Optimized Schwarz methods for advection diffusion equations*
 765 *in bounded domains*, in Numerical Mathematics and Advanced Applications ENUMATH
 766 2017, F. A. Radu, K. Kumar, I. Berre, J. M. Nordbotten, and I. S. Pop, eds., Cham, 2019,
 767 Springer International Publishing, pp. 921–929.
- 768 [19] M. J. GANDER AND Y. XU, *Optimized Schwarz methods for model problems with continuously*
 769 *variable coefficients*, SIAM Journal on Scientific Computing, 38 (2016), pp. A2964–A2986.
- 770 [20] M. J. GANDER AND Y. XU, *Optimized Schwarz methods with nonoverlapping circular domain*
 771 *decomposition*, Mathematics of Computation, 86 (2017), pp. 637–660.
- 772 [21] L. GERARDO-GIORDA, F. NOBILE, AND C. VERGARA, *Analysis and optimization of Robin–Robin*
 773 *partitioned procedures in fluid-structure interaction problems*, SIAM Journal on Numerical

- 774 Analysis, 48 (2010), pp. 2091–2116.
- 775 [22] S.-C. LEE, M. N. VOUVAKIS, AND J.-F. LEE, *A non-overlapping domain decomposition method*
776 *with non-matching grids for modeling large finite antenna arrays*, Journal of Computa-
777 tional Physics, 203 (2005), pp. 1 – 21.
- 778 [23] F. LEMARIÉ, L. DEBREU, AND E. BLAYO, *Toward an Optimized Global-in-Time Schwarz Al-*
779 *gorithm for Diffusion Equations with Discontinuous and Spatially Variable Coefficients,*
780 *Part 1: The Constant Coefficients Case*, Electronic Transactions on Numerical Analysis,
781 40 (2013), pp. 148–169.
- 782 [24] F. LEMARIÉ, L. DEBREU, AND E. BLAYO, *Toward an Optimized Global-in-Time Schwarz Al-*
783 *gorithm for Diffusion Equations with Discontinuous and Spatially Variable Coefficients,*
784 *Part 2: the Variable Coefficients Case*, Electronic Transactions on Numerical Analysis, 40
785 (2013), pp. 170–186.
- 786 [25] P.-L. LIONS, *On the Schwarz alternating method III: a variant for nonoverlapping subdomains*,
787 in Third international symposium on domain decomposition methods for partial differential
788 equations, vol. 6, SIAM Philadelphia, PA, 1990, pp. 202–223.
- 789 [26] Y. MADAY AND F. MAGOULS, *Optimized Schwarz methods without overlap for highly hetero-*
790 *geneous media*, Computer Methods in Applied Mechanics and Engineering, 196 (2007),
791 pp. 1541 – 1553. Domain Decomposition Methods: recent advances and new challenges in
792 engineering.
- 793 [27] V. MARTIN, *Schwarz waveform relaxation method for the viscous shallow water equations*, in
794 Domain Decomposition Methods in Science and Engineering, Berlin, Heidelberg, 2005,
795 Springer Berlin Heidelberg, pp. 653–660.
- 796 [28] F. NATAF, *Absorbing boundary conditions and perfectly matched layers in wave propagation*
797 *problems*, in Direct and Inverse problems in Wave Propagation and Applications, vol. 14
798 of Radon Ser. Comput. Appl. Math., de Gruyter, 2013, pp. 219–231.
- 799 [29] F. NATAF, F. ROGIER, AND E. DE STURLER, *Optimal interface conditions for domain decom-*
800 *position methods*, Tech. report, (1994).
- 801 [30] Z. PENG AND J.-F. LEE, *A scalable nonoverlapping and nonconformal domain decomposition*
802 *method for solving time-harmonic Maxwell equations in r^3* , SIAM Journal on Scientific
803 Computing, 34 (2012), pp. A1266–A1295.
- 804 [31] A. QUARTERONI AND A. VALLI, *Domain Decomposition Methods for Partial Differential Equa-*
805 *tions*, Numerical Mathematics and Scie, Clarendon Press, 1999.
- 806 [32] P. TCHEBYCHEV, *Théorie des mécanismes connus sous le nom de parallélogrammes*, Imprimerie
807 de l’Académie impériale des sciences, 1853.